Quasigeostrophic Forcing of Ascent in the Occluded Sector of Cyclones and the Trowal Airstream

JONATHAN E. MARTIN

Department of Atmospheric and Oceanic Sciences, University of Wisconsin—Madison, Madison, Wisconsin

(Manuscript received 21 October 1997, in final form 27 January 1998)

ABSTRACT

A numerical model-based analysis of the quasigeostrophic forcing for ascent in the occluded quadrant of three cyclones is presented based upon a natural coordinate partitioning of the **Q** vector into its along- and across-isentrope components, $\mathbf{Q}_s$ and $\mathbf{Q}_n$, respectively. The $\mathbf{Q}_n$ component describes the geostrophic contribution to the rate of change of the magnitude of $\nabla_p\theta$ (traditional frontogenesis), whereas the $\mathbf{Q}_s$ component describes the geostrophic contribution to the rate of change of direction of $\nabla_p\theta$ (rotational frontogenesis). It is shown that convergence of $\mathbf{Q}_s$ simultaneously creates the isobaric thermal ridge characteristic of the thermal structure of occluded cyclones and provides the predominant dynamical support for ascent within the occluded quadrant. The absence of significant $\mathbf{Q}_n$ convergence there suggests that quasigeostrophic (Q-G) frontogenesis plays a subordinate role both in forcing vertical motions and in affecting three-dimensional structural changes in the occluded sector of post-mature phase midlatitude cyclones.

A cyclonically ascending, cloud- and precipitation-producing airstream that originates in the warm-sector boundary layer and flows through the trowal portion of the occluded structure is supported by the upward vertical motions implied by the identified Q-G forcing. This airstream is referred to as the ''trowal airstream'' and it is shown to be responsible for the production of the ''wrap around'' cloud and precipitation commonly associated with occluded systems. The relationship of the trowal airstream to previously identified cloud and precipitation producing airflows in cyclones is discussed.

1. Introduction

The relationship between the three-dimensional thermal structure and the distribution of clouds and precipitation in cyclones was first suggested by Bjerknes and Solberg (1922) in their conceptual model of the midlatitude cyclone, which has come to be known as the Norwegian Cyclone Model (NCM). According to their account, the amplification of the cyclone wave distorted the polar front into a cold front and a warm front and left a region of homogeneous warm air extending downward to the surface between the two fronts. This region was known as the warm sector and the air there known as warm sector air.

One of the more intriguing elements of the NCM was the notion of *occluded* fronts first devised by Tor Bergeron (Jewell 1981). Occluded fronts were hypothesized to develop late in the cyclone life cycle and occurred in two varieties: the cold occlusion and the warm occlusion. The warm occlusion described the vertical displacement of warm sector surface air that resulted from the cold front overtaking, and subsequently ascending, the warm frontal surface. One of the main results of this process was the production of a wedge of warm air aloft, displaced poleward of the surface warm and occluded fronts. The cloudiness and precipitation associated with the development of the warm occlusion were suggested to result from lifting of warm air ahead of the upper cold front and were consequently distributed to the north and west of the sea level pressure minimum. Further, as a result of the gradual squeezing of warm air aloft between the two frontal surfaces, the horizontal thermal structure of warm occlusions was characterized by a thermal ridge connecting the peak of the warm sector to the geopotential or sea level pressure minimum. In nature, this thermal ridge is often manifested as a 1000–500-hPa thickness ridge or as an axis of maximum θ or θ_e in a horizontal cross section.

The observation that the cloudiness and precipitation characteristic of the occluded quadrant of cyclones often occurs in the vicinity of the thermal ridge led scientists at the Canadian Meteorological Service (Crocker et al. 1947; Godson 1951; Penner 1955; Galloway 1958, 1960) to regard the essential feature of a warm occlusion to be the trough of warm air that is lifted aloft ahead of the upper cold front, *not* the position of the surface occluded front. These studies suggested that the location

Corresponding author address: Dr. Jonathan E. Martin, Dept. of Atmospheric and Oceanic Sciences, University of Wisconsin—Madison, 1225 W. Dayton St., Madison, WI 53706.
E-mail: jon@meteor.wisc.edu

of a feature called the *trowal* (**tro**ugh of **w**arm air **al**oft) bore a closer correspondence to the cloud and precipitation features of occluded cyclones in North America than did the often weak surface warm occluded front. This relationship was understood, however, in terms of relative flow along the frontal surfaces comprising the occluded structure and not as a consequence of some characteristic dynamical process.

Compelling evidence supporting these observational findings comes from a number of recent finescale numerical modeling studies of occluded cyclones (Schultz and Mass 1993; Reed et al. 1994; Martin 1998a,b) that have illustrated the structure and thermal evolution of, and airflow through, the occluded quadrant. These studies have identified a coherent airstream, originating in the warm sector boundary layer, that ascends cyclonically in the occluded quadrant of the cyclone. Martin (1998b), noting a spatial relationship between the path taken by this airstream and the trowal in his case, referred to this airflow as the ''trowal airstream.'' The results of these model-based analyses have not, however, been fortified by a dynamical explanation of the relationship between the development of the thermal structure in the occluded quadrant of cyclones and the associated ascent that supports this airstream.

In the present paper a quasigeostrophic (Q-G) analysis of the forcing for ascent in the occluded quadrant of three cyclones is presented based upon a partitioning of the **Q** vector (Hoskins et al. 1978) suggested by Kurz (1988b, 1992) and Keyser et al. (1992). It is shown that a single component of the forcing (convergence of the along-isentrope component of **Q**, which represents the rotational component of the quasigeostrophic vector frontogenesis function) simultaneously creates the thermal ridge characteristic of occluded cyclones and provides the vast majority of the Q-G forcing for upward vertical motion within the thermal ridge.

The paper is organized in the following manner. In section 2 a review of the trowal conceptual model and its relationship to the classical warm occlusion is given. The numerical model used to simulate the three cases examined in this work is described in section 3. A model-based synoptic overview of each of the three cases along with selected model-based trajectories for each case are also presented there. In section 4 the quasigeostrophic forcing for ascent in the occluded quadrant of each cyclone is discussed and related to the support of the trowal airstream. A discussion of the importance of the trowal airstream in the midlatitude cyclone and the nature of the vertical motion forcing in the occluded quadrant are given in section 5. A summary and conclusions are offered in section 6.

2. The trowal and its relationship to the warm occlusion

The concept of the trowal was introduced (though not named) by Crocker et al. (1947), who noted the ubiquity of a westward slope to the crests of the thermal wave at successive heights in occluded cyclones. Noting the same feature, Godson (1951) drew attention to its three-dimensional structure by referring to it as a ''sloping valley of tropical air'' (high θ or θ_e) in the occluded quadrant of the cyclone. Penner (1955), who named the feature, stated that the ''trowal marks the crest of the warm air aloft.'' Consistent with each of the above descriptions, the trowal marks the three-dimensional sloping intersection of the upper cold frontal portion of the warm occlusion with the warm frontal zone and could therefore be said to represent a *refined*, three-dimensional description of the warm occluded structure presented by Bjerknes and Solberg (1922) and *not* a new structure. A schematic illustrating the trowal conceptual model is given in Fig. 1.

Consistent with the definition given by Penner (1955) and the description given by Godson (1951), the trowal can be approximately located either as a ridge of high (equivalent) potential temperature on a horizontal cross section, or more precisely located as a three-dimensional sloping canyon in an isosurface of (equivalent) potential temperature. These complementary methods of identifying the trowal are illustrated in Fig. 2 for a case described in detail by Martin (1998a).[1] The relationship of the trowal to the ''wrap around'' cloud and precipitation in occluded cyclones is recognized by some present-day forecasters in Canada. They identify the trowal as the region north and west of the northern edge of the dryslot where the frontal cloud shield of a mature cyclone wraps into the comma head (J. Anderson 1997, personal communication).

Although extensive examination of the trowal was made by the aforementioned Canadian investigators, none of those studies attempted to place this structure in a dynamical context. Morris (1972) identified the trowal as ''a discontinuity in the thermal advection field'' and correctly pointed out that such a feature has dynamical significance with respect to the diagnosis of vertical motion. He employed the traditional quasigeostrophic omega equation to diagnose the vertical motion associated with the trowal portion (i.e., occluded quadrant) of a modest Atlantic cyclone. He ascribed the observed patterns of vertical motion to the influence of the thermal advection term. Martin (1998b) provided evidence that the lower-tropospheric ascent manifested in the trowal airstream in his case was supported by low-level frontogenesis (calculated using the full wind vector) along the warm frontal portion of a warm occluded structure. With the exception of these two cases, no published work has focused on elucidating the dynamical processes responsible for forcing ascent in the

[1] Animation of the 309 K θ_e surface, which demonstrates the structural evolution of the trowal through the cyclone life cycle, can be viewed at the following World Wide Web address: http://marrella.meteor.wisc.edu/occlusion.html.

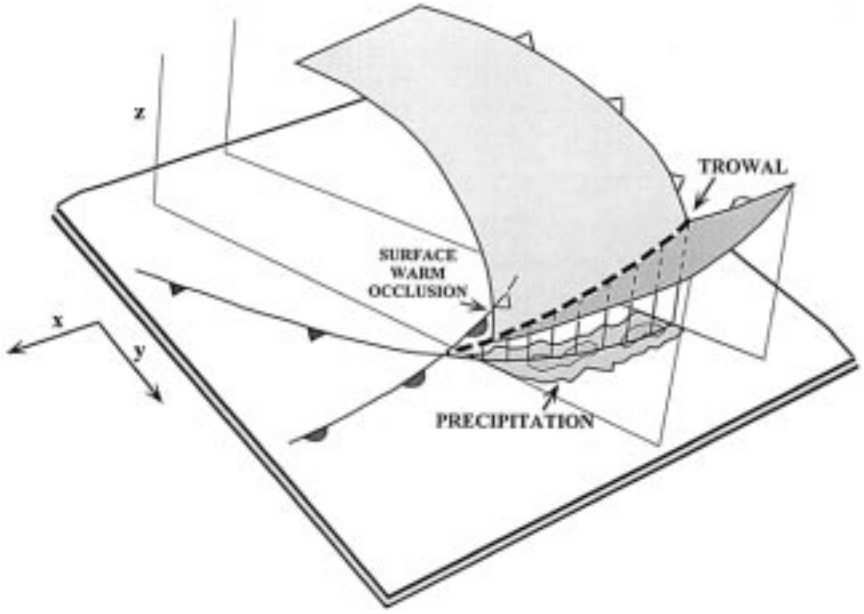

FIG. 1. Schematic illustration of the trowal conceptual model. The lightly shaded surface represents the warm edge of the cold frontal baroclinic zone. The darker shaded surface represents the warm edge of the warm frontal baroclinic zone. The thick dashed line (marked ''TROWAL'') represents the three-dimensional sloping intersection between the cold and warm frontal zones characteristic of warm occlusions. Schematic precipitation band is indicated as are the positions of the surface warm, cold, and occluded fronts.

occluded quadrant of midlatitude cyclones. The present paper offers such a diagnosis of three storms. The diagnosis begins with a synoptic overview of each cyclone given in the next section.

3. Case studies

In this section, three cases of occluded cyclones with trowal structures are briefly described. An overview of the structure of these cyclones, as well as a snapshot of their precipitation distribution is given.[2] The analysis of these cases relied upon a numerical simulation of each performed using the University of Wisconsin-Nonhydrostatic Modeling System (UW-NMS) described by Tripoli (1992a,b).

The model employs a two-way interactive, moveable nesting scheme that allows for the simultaneous simulation of planetary/synoptic-scale forcing as well as frontal-scale forcing. Prognostic variables carried by the model include u, v, w, π (Exner function), ice-liquid potential temperature (θ_{il}), total water mixing ratio, as well as the mixing ratios for a variety of precipitation particles.

Advection of the scalar variables is accomplished using a sixth-order Crowley scheme (Tremback et al. 1987), whereas the dynamic variables are advected using a second-order enstrophy-conserving leapfrog scheme (Sadourny 1975). Model physics include a radiation parameterization that predicts longwave and shortwave radiative transfer in a cloudy atmosphere (Chen and Cotton 1983), and a predictive soil model with surface energy budget (Tremback and Kessler 1985). Liquid and ice processes are represented in the model by an explicit microphysics package, which describes the evolution of cloud water, rainwater, pristine crystals, snow crystals, aggregate crystals, and graupel (Cotton et al. 1986; Flatau et al. 1989). A version of the Emanuel (1991) convective parameterization was employed, modified such that the convection equilibrates with the cyclone and frontal-scale vertical motion forcing.

The two grids used in the simulations had horizontal resolutions of 160 km and 80 km, respectively. Only the 80-km grid data were used in this study. The model employed geometric height as the vertical coordinate with discretely blocked-out topography similar to that used in the National Center for Environmental Prediction's (NCEP's) Eta model. Forty vertical levels were used with the vertical grid spacing of 200 m in the lowest five grid levels and a gradual geometric stretching (by a factor of 1.07) above that such that the next 18 levels had an average spacing of 404 m and the top 17 levels had a spacing of 700 m. The model top was located at 19.2 km.

The model was initialized for each case by interpolating directly from the 90.5-km NCEP Eta initializa-

[2] Radar reflectivity data were not available for the 7 November 1996 case.

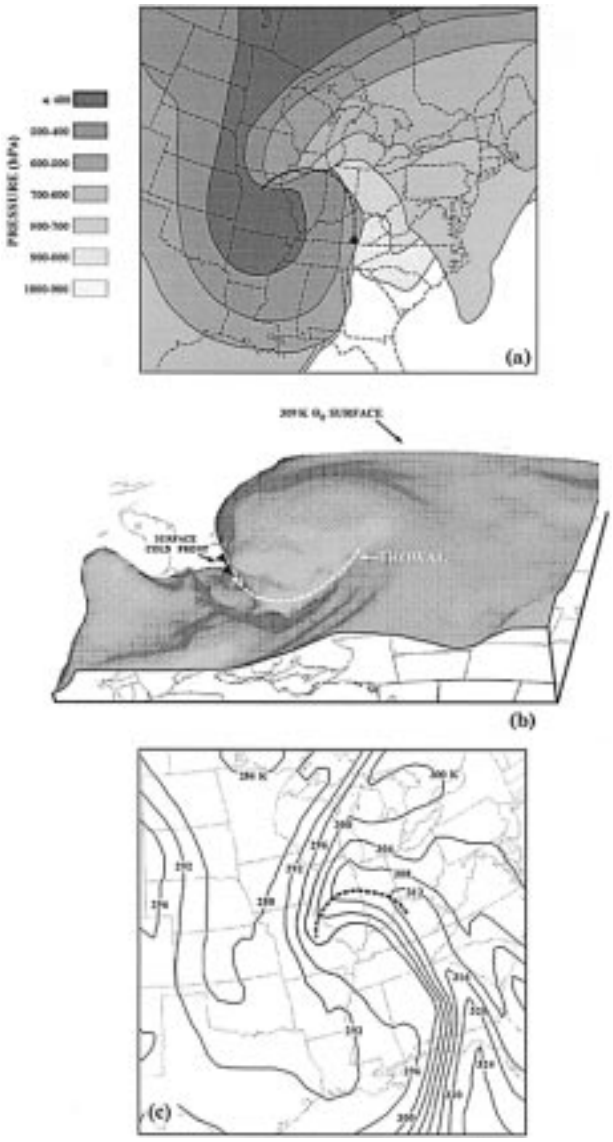

FIG. 2. (a) Isobaric topography of the 309 K θ_e surface from an 18-h forecast of the University of Wisconsin-Nonhydrostatic Modeling System valid at 1800 UTC 19 January 1995. Shading depicts isobaric levels at 100-hPa intervals with lightest shading representing the 1000–900-hPa layer and darkest shading representing the layer above 400 hPa. Thick solid/dashed line is plan view of the trowal position, dashed to indicate where the 309 K θ_e surface overhangs the trowal location. (b) Elevated view from the north of the 309 K θ_e surface from an 18-h forecast of the UW-NMS valid at 1800 UTC 19 January 1995. The dashed line indicates the trowal position, which slopes upward from near the surface to ~8 km. Position of the surface cold front is also indicated. (c) Equivalent potential temperature at 2 km from an 18-h forecast of the UW-NMS valid at 1800 UTC 19 January 1995. Solid lines are θ_e, labeled in K and contoured every 4 K. Thick dashed line is the axis of maximum θ_e characteristic of a warm occluded cyclone and used to approximately locate the trowal.

tion, which has 50-hPa vertical resolution. Horizontal wind components, geopotential height, temperature, and relative humidity were interpolated horizontally along constant pressure surfaces to the locations of the model grid points. Data were then vertically interpolated to the model grid levels. The lateral boundaries were updated every 6 h from the Eta gridded forecasts using a Rayleigh-type absorbing layer. In all three cases, 36-h simulations were employed in order to keep the output visualization datasets at a manageable size. Twelve and 18-h forecast data were used in the study (as opposed to 0- and 6-h forecasts) to ensure that the occluded structures present in each case developed within the model simulation.

Air parcel trajectories were calculated using u, v, and w from the model output, using a forward differencing scheme with a time step of 24.5 min. Additional analysis of these data was performed using the General Meteorological Analysis Package. Brief descriptions of each of the three cases used in this study are given below.

a. 23 October 1996

At 0600 UTC 23 October 1996, an occluded surface low pressure center with a sea level pressure minimum of 992 hPa was located over east-central Iowa. A fairly well defined axis of maximum surface θ extended from extreme northeast Iowa south-southwestward into north-central Missouri (Fig. 3a). The geopotential minimum at 850 hPa was centered in southeast Iowa (Fig. 3b) with an associated axis of maximum θ located in roughly the same geographic area as, although more elongated than, its surface counterpart. The geopotential minimum axis tilted to the south-southwest with height. The axes of maximum θ in the middle troposphere were not nearly as well defined as at lower tropospheric levels, as evidenced by the weaker axis of high θ at 700 hPa (Fig. 3c) that extended from northcentral Wisconsin to northwest Missouri. Nonetheless, these thermal axes exhibited a northwestward tilt with height. An axis of maximum θ was barely detectable at 500 hPa (Fig. 3d).

A vertical cross section through the occluded portion of this cyclone (not shown) revealed the 315 K θ_e surface to be appropriate for further analysis of the trowal structure. The isobaric topography of that surface is given in Fig. 4a. The trowal position, identified by connecting the crests of the various isobaric surfaces in the ridge of high pressure, stretched from the Iowa/Minnesota/Wisconsin border southwestward to south of Kansas City, Missouri. An elevated, northern view of the 315 K θ_e surface offers another perspective of the trowal structure in this case (Fig. 4b). The unusual extent of the ''wrap around'' precipitation exhibited by this storm (Fig. 4c) was directly related to ascent in the trowal portion of the cyclone (to be shown later). In fact, between Omaha, Nebraska, and Kansas City, Missouri, the precipitation fell in the form of snow and provided that area with its most significant early season snowstorm in history (National Climatic Data Center 1996).

Of the several coherent airstreams subjectively identified in this case through use of model-based trajectory

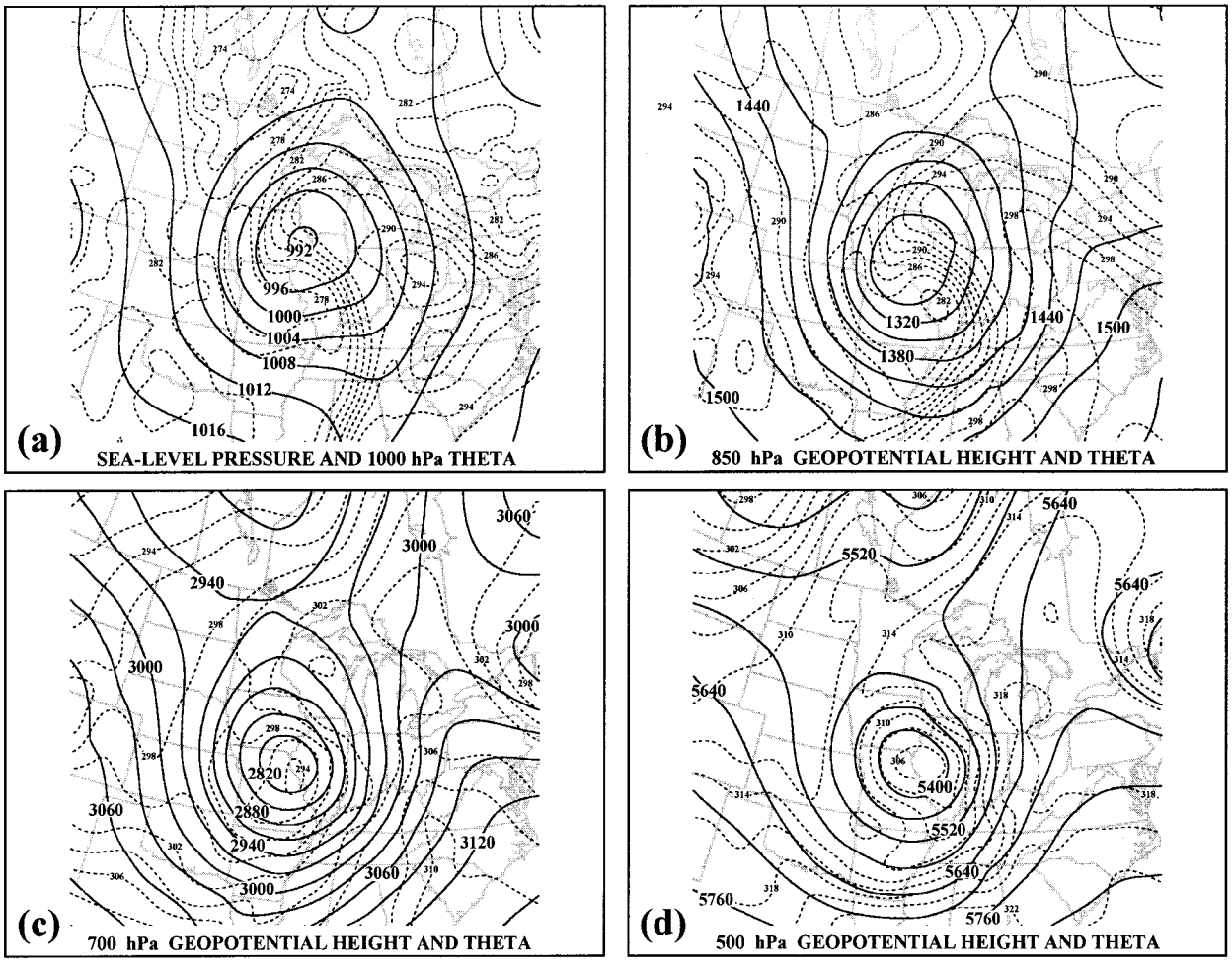

FIG. 3. (a) Sea level isobars (solid lines) and 1000-hPa potential temperature (dashed lines) from an 18-h forecast of the UW-NMS valid at 0600 UTC 23 October 1996. Isobars are labeled in hPa and contoured every 4 hPa. Isentropes are labeled in K and contoured every 2 K. (b) 850-hPa geopotential height (solid lines) and potential temperature (dashed lines) from an 18-h forecast of the UW-NMS valid at 0600 UTC 23 October 1996. Geopotential height labeled in m and contoured every 30 m. Potential temperature analyzed as in Fig. 3a. (c) As for Fig. 3b except for 700 hPa. (d) As for Fig. 3b except for 500 hPa with geopotential height contoured every 60 m.

analysis, two are highlighted in Fig. 5. Trajectory B is representative of an airstream that originated east of the surface cold front in the warm sector boundary layer. It surged northward in a low-level jet and rose abruptly upon becoming incorporated into a vigorous squall line. As it rose it turned anticyclonically thus fitting the description of the warm conveyor belt (Browning and Harrold 1969; Harrold 1973; Carlson 1980). Trajectory A is representative of an airstream that also originated in the warm sector boundary layer. It was extremely moist (mixing ratio of 11 g kg^{-1} initially) and it surged northward east of the surface cold front as well. However, this airstream was not involved in the squall line as parcels transported within it had moved too far north by the time the squall line became organized. Instead, this airstream rose gently until reaching the trowal (~0600 UTC 23 October) at which time it commenced a rapid, cyclonic ascent in the trowal.[3] Trajectory A represents the trowal airstream in this cyclone.

b. 7 November 1996

At 1200 UTC 7 November 1996, a surface low pressure center with a minimum sea level pressure of 987 hPa was located in central Ontario at the crest of a ridge of high surface θ (Fig. 6a). The geopotential minimum at 850 hPa was located directly atop the center of the surface disturbance (Fig. 6b). A ridge of high θ at that

[3] Combined animation of this airstream and the 315 K θ_e surface for this cyclone, with similar animations of the other two storms reviewed here, is available for inspection at the following World Wide Web address: http://marrella.meteor.wisc.edu/trowal.html.

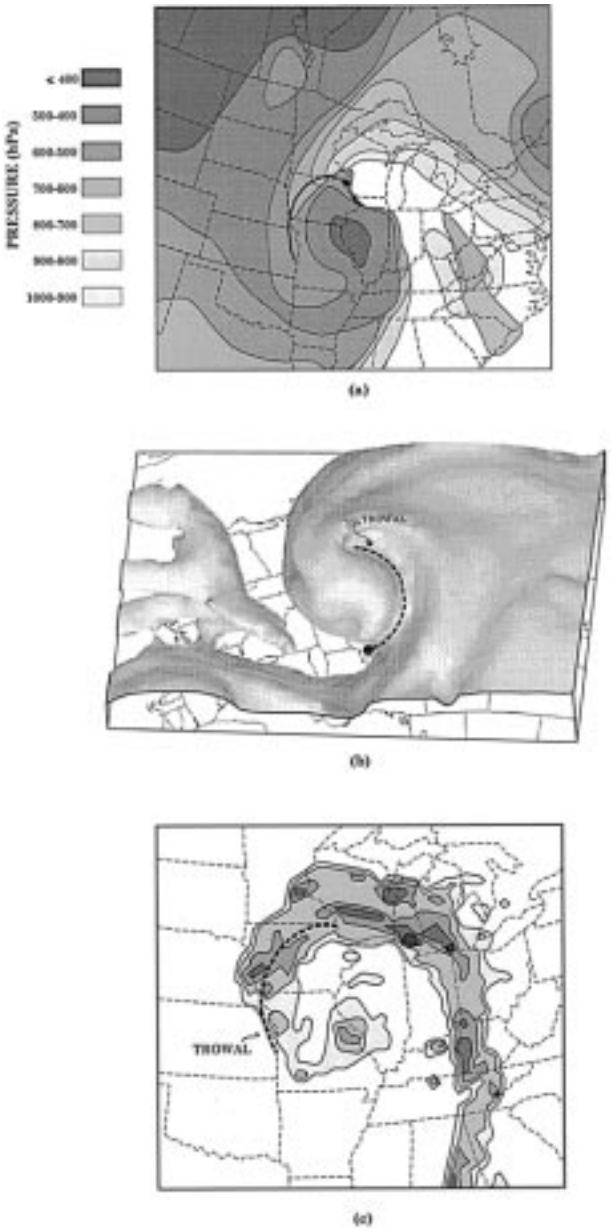

FIG. 4. (a) Isobaric topography of the 315 K θ_e surface from an 18-h forecast of the UW-NMS valid at 0600 UTC 23 October 1996. Isobaric layers shaded and contoured, and trowal position indicated, as in Fig. 2a. (b) Elevated, northern perspective of the 315 K θ_e surface from an 18-h forecast of the UW-NMS valid at 0600 UTC 23 October 1996. Dashed line indicates trowal position, which slopes upward from the surface to ~6 km. (c) National Weather Service (NWS) manually digitized radar reflectivity at 0635 UTC 23 October 1996. Shading indicates echo/precipitation rate intensity from level 1 to level 5 signifying light, moderate, heavy, very heavy, and intense precipitation, respectively. Thick dashed line indicates trowal position as shown in Figs. 4a and 4b.

level extended through the geopotential minimum in a semicircle from near James Bay, Ontario, to southcentral Ontario. As in the previous case, the axis of geopotential minima tilted southward with height as evidenced by

FIG. 5. Representative 27-h forward trajectories originating in the warm sector boundary layer at 1200 UTC 22 October 1996 calculated from the UW-NMS model data. Width of the trajectory arrow indicates height of the air parcel according to the legend. Tick marks on trajectory arrows represent 3-hourly positions of air parcels. See text for discussion of A and B.

the position of the geopotential minimum at 700 hPa (Fig. 6c) and 500 hPa (Fig. 6d). More importantly, at these midtropospheric levels the ridge of high θ was located progressively farther north and west.

Vertical cross section analyses (not shown) revealed the 309 K θ_e surface to be near the warm edge of both the cold and warm frontal zones in the occluded portion of this cyclone. The isobaric topography of the 309 K θ_e surface at 1200 UTC 7 November is shown in Fig. 7a. Based upon this analysis, the trowal position stretched from north of Lake Huron through James Bay to northwest Ontario. An elevated eastern perspective of the 309 K θ_e surface (Fig. 7b) clearly demonstrates the three-dimensional nature of the trowal structure as a ''sloping valley'' of high θ_e air. The position of the trowal bears an obvious relationship to the UW-NMS forecasted 1-h precipitation total ending at this time (Fig. 7c).

Of the several coherent airstreams subjectively identified in this storm through use of model-based trajectory analysis, two are presented in Fig. 8. Trajectory B is representative of an airstream that originated in the lower troposphere (~1.7 km) east of the cold frontal zone. This airstream rose only slightly until encountering the warm frontal zone at which time it rose abruptly to ~7 km. Trajectory A is representative of an airstream that also originated east of the cold frontal zone in the lower troposphere (~1.5 km). This airstream rose gently until encountering the lower portion of the trowal (~1200 UTC 7 November) after which time it began a rapid, cyclonically turning ascent through the occluded quadrant of the storm. Trajectory A represents the trowal airstream in this cyclone.

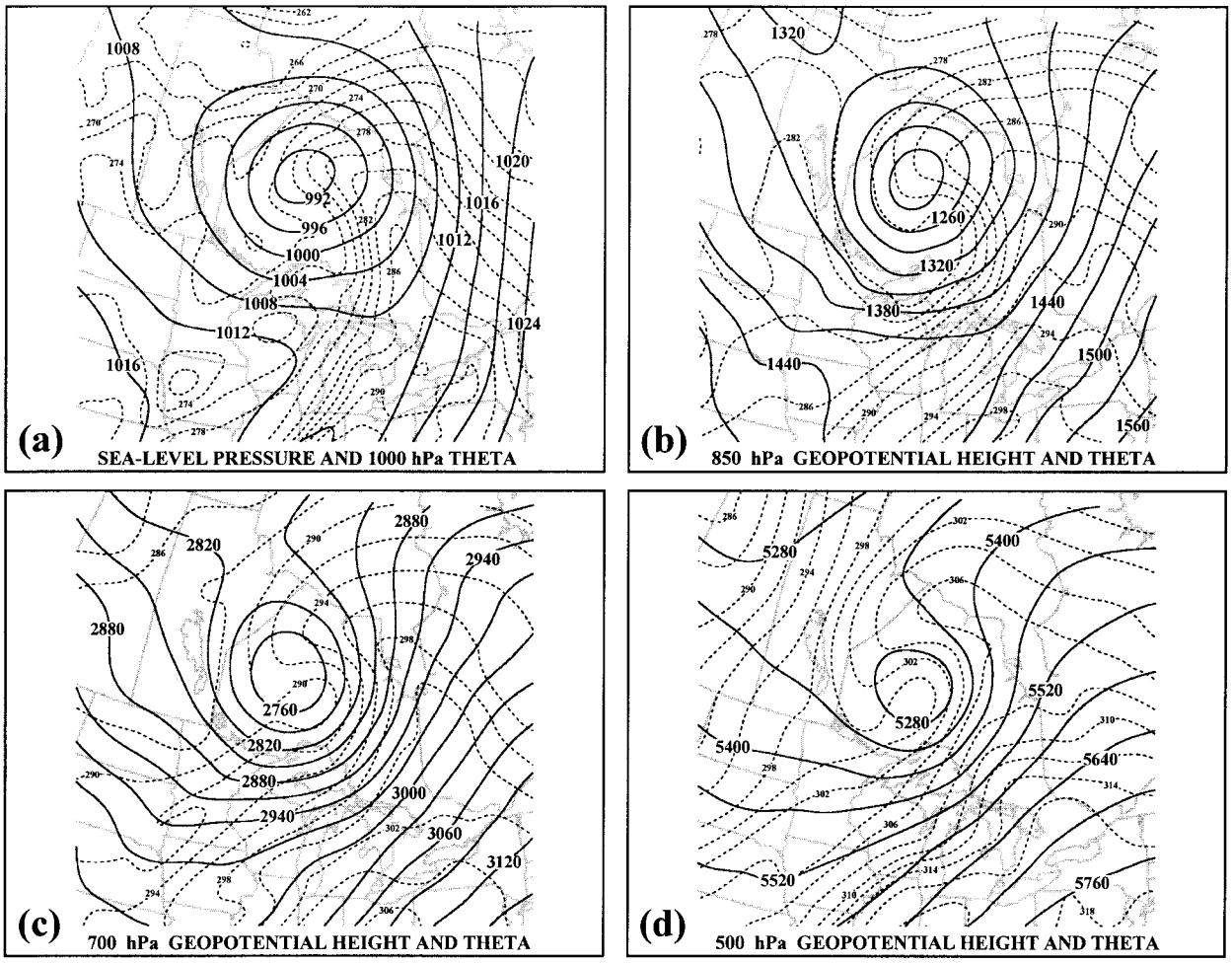

FIG. 6. (a) As for Fig. 3a except for 12-h forecast from UW-NMS valid at 1200 UTC 7 November 1996. (b) As for Fig. 3b except for 12-h forecast from UW-NMS valid at 1200 UTC 7 November 1996. (c) As for Fig. 3c except for 12-h forecast from UW-NMS valid at 1200 UTC 7 November 1996. (d) As for Fig. 3d except for 12-h forecast from UW-NMS valid at 1200 UTC 7 November 1996.

c. 1 April 1997

One of the most memorable snowstorms in the history of southern New England occurred on 31 March–1 April 1997. At 0600 UTC 1 April, a surface low pressure center was located ~400 km south of Nantucket, Massachusetts, and had a minimum sea level pressure of 981 hPa (Fig. 9a). A secondary surface cold front existed along the Atlantic Coast of the United States, whereas the primary surface cold front associated with this cyclone was well to the east out to sea. The surface warm front, located south of Nova Scotia at this time, was a robust feature of this cyclone.

The geopotential minimum at 850 hPa was located directly above the surface disturbance (Fig. 9b). The primary cold frontal zone was more vigorous at this level than at the surface. The secondary cold frontal zone off the Carolina coast along with the warm frontal zone south of Nova Scotia were also well defined at this level. An incipient axis of high θ was also evident at 850 hPa extending from south of Nova Scotia to south of Long Island.

Even more dramatic distortion of the baroclinic zone associated with this cyclone was evident at 700 hPa where the ridge of high θ extended cyclonically from just south of Nova Scotia westward across southern New England and southward to the west of the geopotential minimum, which was located directly above its 850-hPa counterpart (Fig. 9c). The primary cold frontal zone was even stronger at this level than at 850 hPa, whereas the warm frontal zone was more diffuse. No evidence of the lower-tropospheric secondary cold front existed at 700 hPa.

At 500 hPa (Fig. 9d) an extraordinarily lengthy axis of maximum θ was evident from the Gulf of Maine, through southern New England, and southward to Chesapeake Bay. An intense baroclinic zone bordered the geopotential height minimum at this level, particularly on its southern and eastern edges.

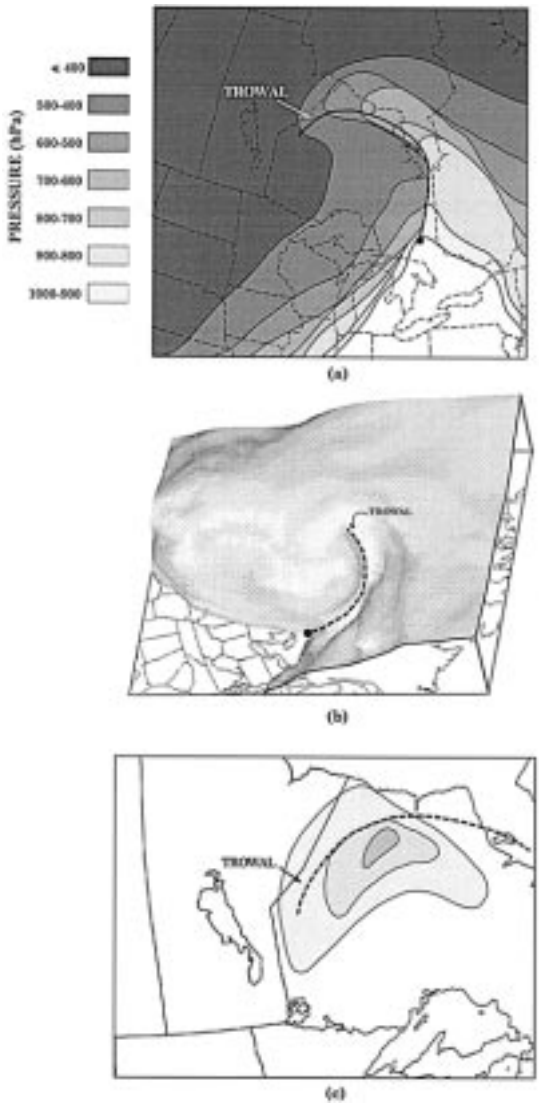

FIG. 7. Isobaric topography of the 309 K θ_e surface from a 12-h forecast of the UW-NMS valid at 1200 UTC 7 November 1996. Pressure layers shaded and contoured, and trowal position indicated, as in Fig. 2a. (b) Elevated, eastern view of the 309 K θ_e surface from a 12-h forecast of the UW-NMS valid at 1200 UTC 7 November 1996. Thick dashed line indicates the trowal position. (c) Forecast of accumulated 1-h liquid equivalent precipitation ending at 1200 UTC 7 November 1996 from the UW-NMS. Precipitation totals are contoured and shaded every 1 mm (beginning at 1 mm). Thick dashed line indicates trowal position as determined in Figs. 7a and 7b.

Vertical cross sections through the ridge of high θ (not shown) revealed that the 312 K θ_e surface formed the warm edges of both the cold and warm frontal portions of the warm occluded structure of this storm. The location of the trowal was determined by considering the topography of the 312 K θ_e surface. A plain view of the isobaric topography of this θ_e surface is shown in Fig. 10a. As in the previous cases, the trowal position was determined by connecting the crests of the various isobaric surfaces in the ridge of high pressure and was thus placed on a cyclonically curving line that stretched from well south of Nova Scotia through southern New England at this time.

FIG. 8. Representative 24-h forward trajectories initialized in the warm sector boundary layer at 0000 UTC 7 November 1996. Width of the trajectory arrow indicates height of the air parcel according to the legend. Tick marks on trajectory arrows represent 3-hourly positions of air parcels. See text for discussion of A and B.

An elevated, northeastern view of this three-dimensional moist isentropic surface provides a different perspective of the structure of the trowal in this cyclone (Fig. 10b). Although radar coverage was limited offshore, a widespread region of precipitation was occurring from southeast Maine southwestward to the Delmarva peninsula at this time in association with ascent in the trowal portion of the cyclone (Fig. 10c).

Two representative trajectories involved in the production of clouds and precipitation in this cyclone are shown in Fig. 11. Trajectory B originated at low levels in the warm sector and remained below 1 km until encountering the surface warm front at ~0000 UTC 1 April. After this time trajectory B rose abruptly to 6.6 km as a portion of the warm conveyor belt airstream responsible for producing the eastern portion of the cyclone comma head cloud shield (not shown). Trajectory A, the trowal airstream in this cyclone, originated ~200 m above the surface in the warm sector and had a mixing ratio of 12 g kg^{-1} at its origin. It also remained quasi-horizontal until ~0000 UTC 1 April at which time it began a rapid ascent in the trowal to ~7 km. The enormous snowfall totals that visited many locations in the northeastern United States in association with this spring in blizzard (National Climatic Data Center 1997a,b) were a direct result of the rapid ascent of the trowal airstream associated with this cyclone.

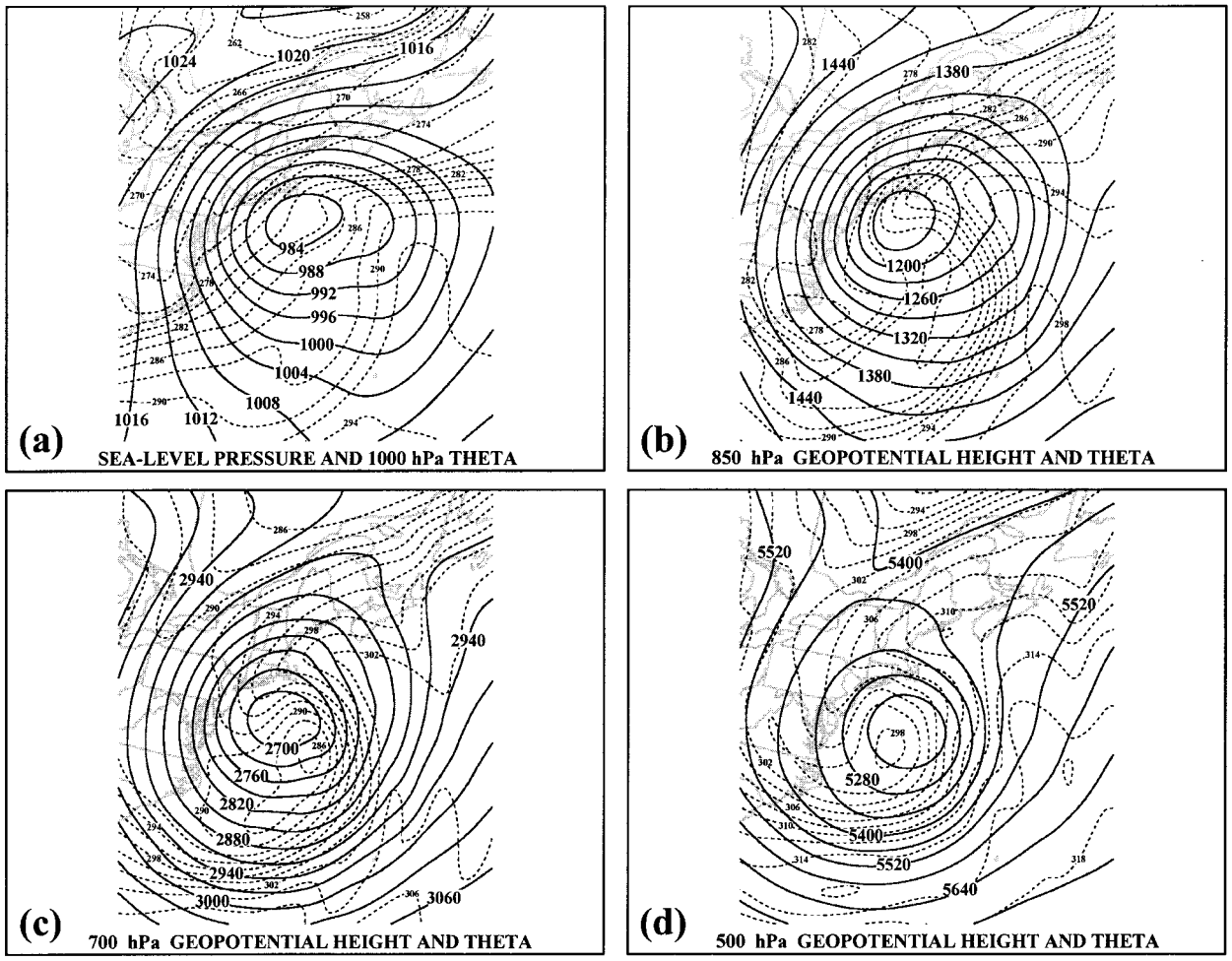

FIG. 9. (a) As for Fig. 3a except for 18-h forecast from UW-NMS valid at 0600 UTC 1 April 1997. (b) As for Fig. 3b except for 18-h forecast from UW-NMS valid at 0600 UTC 1 April 1997. (c) As for Fig. 3c except for 18-h forecast from UW-NMS valid at 0600 UTC 1 April 1997. (d) As for Fig. 3d except for 18-h forecast from UW-NMS valid at 0600 UTC 1 April 1997.

4. Quasigeostrophic forcing of ascent in the vicinity of the trowal

In the previous section, three cases were described in which a coherent airstream underwent ascent, while turning cyclonically, in the vicinity of the trowal. The ascent manifested in these important precipitation producing airstreams was a result of the distribution of vertical motion accompanying the individual cyclones. In this section, a quasigeostrophic diagnosis of the forcing for the supporting vertical motions is undertaken by examining the divergence of the **Q** vector (Hoskins et al. 1978) and considering its decomposition in relation to the horizontal potential temperature gradient.

a. The quasigeostrophic omega equation

The diagnosis of vertical motions on the synoptic scale is made possible through use of the quasigeostrophic (Q-G) omega equation:

$$\left(\sigma\nabla^2 + f_o^2\frac{\partial^2}{\partial p^2}\right)\omega = f_o\frac{\partial}{\partial p}\left[\mathbf{V}_g\cdot\boldsymbol{\nabla}\left(\frac{1}{f_o}\nabla^2\phi + f\right)\right] + \nabla^2\left[\mathbf{V}_g\cdot\boldsymbol{\nabla}\left(-\frac{\partial\phi}{\partial p}\right)\right] \quad (1)$$

(Holton 1992). As demonstrated by Trenberth (1978), some cancellation exists between the two terms on the rhs of (1). By expanding the expressions on the rhs of (1) and neglecting the deformation term, Trenberth arrived at the following approximate f-plane form of the Q-G omega equation,

$$\left(\sigma\nabla^2 + f_o^2\frac{\partial^2}{\partial p^2}\right)\omega \approx \mathrm{F_{TR}} = 2f_o\mathbf{V}_T\cdot\boldsymbol{\nabla}\zeta_g, \quad (2)$$

where $\mathbf{V}_T$ is the thermal wind ($\partial\mathbf{V}_g/\partial p$) and ζ_g is the geostrophic relative vorticity. This relationship, in which synoptic-scale vertical motion is controlled by

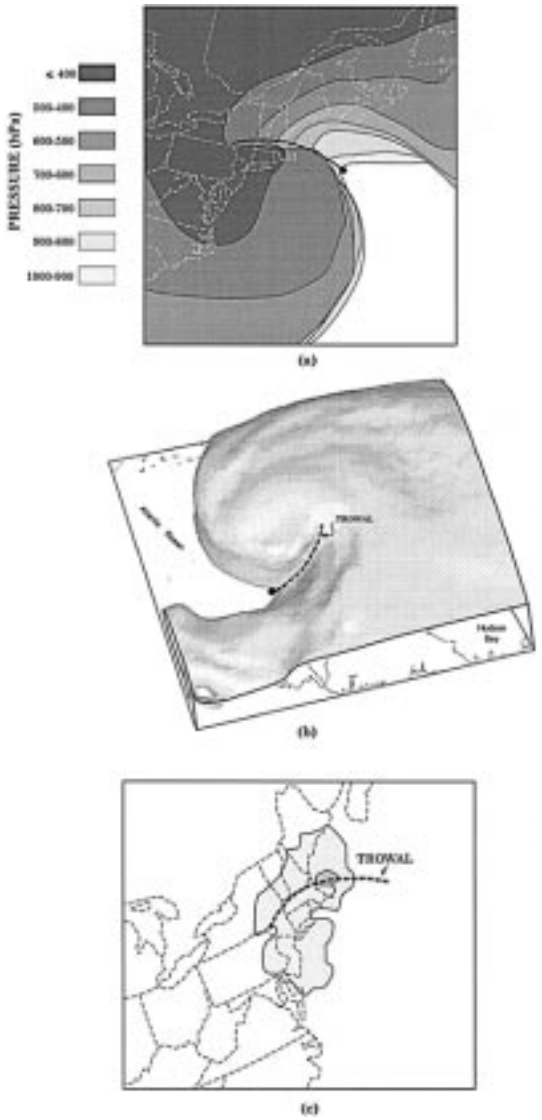

FIG. 10. (a) Isobaric topography of the 312 K θ_e surface from an 18-h forecast of the UW-NMS valid at 0600 UTC 1 April 1997. Pressure levels shaded and contoured, and trowal position indicated, as in Fig. 2a. (b) Elevated, northeastern perspective of the 312 K θ_e surface from an 18-h forecast of the UW-NMS valid at 0600 UTC 1 April 1996. Thick dashed line indicates the trowal position, which slopes upward from the surface to ~8 km. (c) As for Fig. 4c but for 0635 UTC 1 April 1997.

the advection of geostrophic relative vorticity by the thermal wind, is a close relative of the development equation forwarded by Sutcliffe (1947). Both the Sutcliffe (1947) and Trenberth (1978) versions of (1) retain their simplified forms at the expense of neglecting terms involving the deformation of the horizontal flow. Deformation is important in baroclinic regions, such as fronts, and thus, potentially important information regarding omega is lost in these simplified expressions.

Hoskins and Pedder (1980) showed that F_{TR} could be written in a vector divergence form as

FIG. 11. Representative 24-h forward trajectories initialized in the warm sector boundary layer at 1200 UTC 31 March 1997 from the UW-NMS. Height of air parcels indicated by width of trajectory arrow according to legend. Tick marks identify 3-hourly positions of air parcels. See text for discussion of A and B.

$$F_{TR} = -2\nabla \cdot \mathbf{Q}_{TR}, \tag{3}$$

where $\mathbf{Q}_{TR} = f_o \gamma \zeta_g (\hat{\mathbf{k}} \times \nabla\theta)$ and

$$\gamma = \frac{R}{f_o P_o}\left(\frac{P_o}{P}\right)^{c_v/c_p}$$

and is constant on isobaric surfaces. This form of F_{TR}, where the forcing depends on the convergence of a vector field that is everywhere parallel to the (layer mean) isentropes, demonstrates that this forcing can never be distributed in bands parallel to the isentropes. Thus, it does not describe the forcing of banded vertical motions parallel to baroclinic zones such as occurs at fronts. The Trenberth forcing, therefore, could be said to describe only the nonfrontal, synoptic-scale forcing for Q-G vertical motion.

A complete solution to the Q-G omega equation was introduced by Hoskins et al. (1978). They showed that the synoptic-scale vertical motion is controlled by the divergence of the **Q** vector defined as

$$\mathbf{Q} = -f_o \gamma \left[\left(\frac{\partial \mathbf{V}_g}{\partial x} \cdot \nabla\theta\right)\hat{\mathbf{i}} + \left(\frac{\partial \mathbf{V}_g}{\partial y} \cdot \nabla\theta\right)\hat{\mathbf{j}}\right]. \tag{4}$$

For adiabatic, geostrophic flow, the **Q** vector represents the rate of change of the vector $\nabla_p\theta$ along a geostrophic trajectory:

$$\mathbf{Q} = f_o \gamma \frac{d}{dt_g}\nabla_p\theta, \tag{5}$$

where $d/dt_g = \partial/\partial t + \mathbf{V}_g \cdot \nabla_p$ (the subscript g denotes

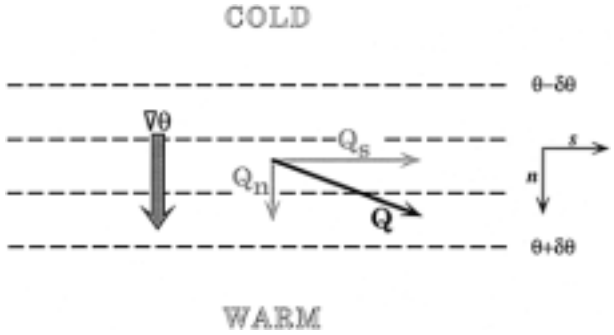

FIG. 12. Schematic describing the natural coordinate partitioning of the **Q** vector used in this study. Thick dashed lines are isentropes on an isobaric surface. Here $\mathbf{Q}_n$ ($\mathbf{Q}_s$) is the component of **Q** in the $\hat{\mathbf{n}}$ ($\hat{\mathbf{s}}$) direction.

geostrophic). As a result, the **Q** vector contains information about both the rate of change of the *magnitude* of $\nabla_p\theta$ (the traditional parameter examined in frontogenesis calculations) and the rate of change of the *direction* of the vector $\nabla_p\theta$. In an effort to exploit this definition of the **Q** vector, Keyser et al. (1992), following a suggestion by Keyser et al. (1988), partitioned the **Q**-vector field into natural coordinate components in directions along ($\mathbf{Q}_s$) and across ($\mathbf{Q}_n$) the isentropes. Physically, $\mathbf{Q}_n$ and $\mathbf{Q}_s$ represent the *magnitude* and *rotational* components of the Q-G vector frontogenesis, respectively. A similar partitioning formed the basis of studies by Kurz (1988b, 1992).

Our vector decomposition of the **Q**-vector components along the direction of the potential temperature gradient vector ($\hat{\mathbf{n}}$) and 90° counterclockwise from that direction ($\hat{\mathbf{s}}$) ($\hat{\mathbf{s}} = \hat{\mathbf{k}} \times \hat{\mathbf{n}}$) [which is different from that employed by Keyser et al. (1992)] is illustrated with the aid of Fig. 12. The unit vector in the direction of $\nabla\theta$ is given by

$$\hat{\mathbf{n}} = \frac{\nabla\theta}{|\nabla\theta|}. \tag{6}$$

The component of **Q** in the direction of $\hat{\mathbf{n}}$ will be denoted as $\mathbf{Q}_n$ and is equal to

$$\mathbf{Q}_n = \left(\frac{\mathbf{Q}\cdot\nabla\theta}{|\nabla\theta|}\right)\frac{\nabla\theta}{|\nabla\theta|} \quad \text{or} \quad \mathbf{Q}_n = \left(\frac{\mathbf{Q}\cdot\nabla\theta}{|\nabla\theta|}\right)\hat{\mathbf{n}}. \tag{7}$$

Recalling that the Q-G frontogenesis function is given by

$$\mathrm{F}_g = \left(\frac{\mathbf{Q}\cdot\nabla\theta}{|\nabla\theta|}\right)$$

(Hoskins and Pedder 1980), the expression for $\mathbf{Q}_n$ reduces to $\mathbf{Q}_n = \mathrm{F}_g\hat{\mathbf{n}}$. Thus, $\mathbf{Q}_n$ is large (small) where $\mathbf{F}_g$ is large (small).

Based on their examination of the generalized Petterssen frontogenesis function, Keyser et al. (1988) proposed, and Keyser et al. (1992) demonstrated, that the Q-G forcing of vertical motion associated with $\mathbf{Q}_n$ (i.e., $-2\nabla\cdot\boldsymbol{Q}_n$) forces elongated, banded regions of vertical motion that are parallel to, associated with, and distributed along the warm edges of regions of concentrated baroclinicity (frontal zones) within the flow. In examinations of real cyclone events, Kurz (1992) and Barnes and Colman (1993) offered support for this assertion. Given the dependence of $\mathbf{Q}_n$ on F_g, it is not surprising that this across-isentrope component of **Q** relates to the forcing of vertical motion associated with frontogenetic processes. It follows that if the baroclinic zones bordering the occluded thermal ridge are both characterized by positive Q-G frontogenesis, then the thermal ridge will be characterized by significant $\mathbf{Q}_n$ convergence and frontogenetically forced ascent.

The component of **Q** along the isentropes will be denoted as $\mathbf{Q}_s$ and is equal to

$$\mathbf{Q}_s = \frac{\mathbf{Q}\cdot(\hat{\mathbf{k}}\times\nabla\theta)}{|\nabla\theta|}\left[\frac{(\hat{\mathbf{k}}\times\nabla\theta)}{|\nabla\theta|}\right]. \tag{8}$$

Keyser et al. (1988) demonstrated that, following the geostrophic flow, the potential temperature gradient vector is rotated in the direction of $\mathbf{Q}_s$ to a degree proportional to the magnitude of $\mathbf{Q}_s$ (the reader is referred to that work for the complete derivation of this relationship). As a result, the $\mathbf{Q}_s$-component of the **Q** vector exerts a considerable influence on the evolution of the characteristic occluded thermal structure. This important point is illustrated schematically in Fig. 13 where an originally straight-line baroclinic zone is characterized by $\mathbf{Q}_s$ convergence. The $\mathbf{Q}_s$ vectors located to the left (right) of the $\mathbf{Q}_s$ convergence maximum in Fig. 13a describe the geostrophic contribution to counterclockwise (clockwise) rotation of the $\nabla_p\theta$ vector with time. This differential rotation on opposite sides of the $\mathbf{Q}_s$-convergence maximum produces a thermal ridge in the horizontal while simultaneously providing Q-G forcing for upward vertical motion within that thermal ridge (Fig. 13c). Thus, the same Q-G forcing that aids in the production of this characteristic horizontal thermal structure also provides forcing for upward vertical motions in the occluded quadrant of cyclones.

Employing output from a nearly adiabatic and frictionless, primitive equation channel model of the evolution of a baroclinic cyclone, Keyser et al. (1992) found that the pattern of vertical motion associated with $-2\nabla\cdot\mathbf{Q}_s$ was cellular and occurred on the synoptic scale, the scale of the baroclinic disturbance (which they termed *wave scale*). A similar result was reported by Kurz (1992). In the following subsections comparison between the Trenberth and partitioned **Q**-vector forcings for Q-G vertical motion in the vicinity of the trowal will show that ascent in the occluded quadrant of cyclones is predominantly forced by $\mathbf{Q}_s$ convergence and is therefore largely a result of synoptic-scale dynamical processes.

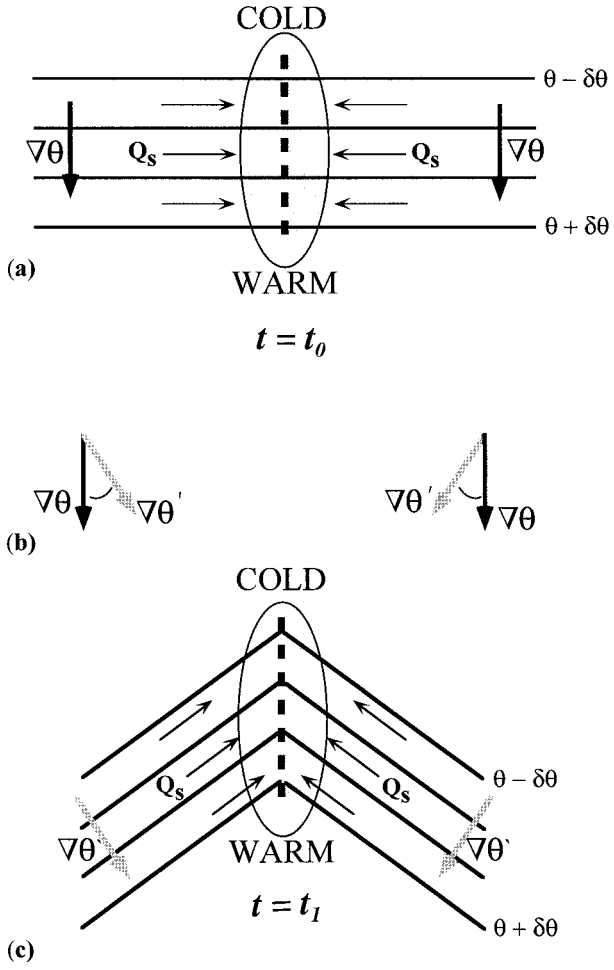

FIG. 13. The effect of $\mathbf{Q}_s$ convergence on horizontal thermal structure. (a) Straight line isentropes (solid lines) in a field of $\mathbf{Q}_s$ convergence (shading). Thick dashed line indicates axis of maximum $\mathbf{Q}_s$ convergence. Direction of $\nabla\theta$ vector on either side of the $\mathbf{Q}_s$ convergence maximum is indicated. (b) Rotation of $\nabla\theta$ vector implied by $\mathbf{Q}_s$ vectors on either side of the $\mathbf{Q}_s$ convergence maximum in Fig. 13a. Thick black arrow denoted as $\nabla\theta$ represents original direction of $\nabla\theta$ vector. Thick gray arrow denoted as $\nabla\theta'$ represents direction of $\nabla\theta$ vector after rotation implied by $\mathbf{Q}_s$ vectors. (c) Orientation of the baroclinic zone depicted in Fig. 13a after differential rotation of $\nabla\theta$ on either side of the $\mathbf{Q}_s$ convergence maximum.

b. 23 October 1996

Since the trowal structure, as identified from analyses of θ_e presented earlier, did not extend above ~5 km at 0600 UTC 23 October 1996, analyses of the Q-G forcing in the 600–900-hPa layer at this time are presented. The Trenberth forcing function in this layer at this time [calculated using (2) and the average geostrophic relative vorticity in the given layer] is shown in Fig. 14a along with the column-averaged isentropes in the layer. Only one significant feature appears in the forcing, namely the axis of large forcing that extends from near Minneapolis, Minnesota, to northcentral Missouri, immediately west of the axis of high column-averaged θ. This axis is nearly collocated with the trowal identified in Fig. 3.

The total column-averaged **Q** vectors and their convergence are shown in Fig. 14b. The area of large forcing in the vicinity of the trowal is one of two major features. A second feature of importance is the axis of significant forcing that extends from near Indianapolis southward to northern Georgia. This latter feature was collocated with the lower-tropospheric cold frontal zone (Fig. 3a). Smaller-scale regions of forcing in central Alabama and along the Mississippi/Alabama border are common to Figs. 14a and 14b.

The $\mathbf{Q}_s$ vectors and their convergence in the 600–900-hPa layer at 0600 UTC 23 October are shown in Fig. 14c. The distribution of this component of the **Q**-vector forcing resembles that of the synoptic-scale (Trenberth) forcing shown in Fig. 14a. The trowal, as identified in Fig. 4a, lies just to the north and west of the axis of maximum $\mathbf{Q}_s$ forcing for vertical motion, which contributes nearly all of the Q-G forcing for vertical motion in the occluded quadrant of the cyclone. The previously identified smaller-scale features in the Trenberth and total **Q**-vector forcing (in Mississippi and Alabama) are also evident in the convergence of $\mathbf{Q}_s$. It is important to note that since $\hat{\mathbf{s}}$ changes direction along isotherms, $\nabla \cdot \hat{\mathbf{s}}$ can contribute to $\nabla \cdot \mathbf{Q}_s$. Calculations of this effect (not shown) revealed that in this case, as well as in the other two, the unit vector contribution to $\mathbf{Q}_s$ convergence was negligible (i.e., at least one order of magnitude smaller) or of opposite sign in regions of $\mathbf{Q}_s$ convergence.

The $\mathbf{Q}_n$ component of **Q** and its convergence in the 600–900-hPa layer are shown in Fig. 14d. The most potent feature in this convergence field is the banded forcing extending from Indianapolis to northern Alabama. This feature represents the forcing associated with the frontogenesis along the lower-tropospheric cold front. The strip of weaker $\mathbf{Q}_n$ forcing that stretched from northwest Ohio to central Wisconsin was located within the weak eastern portion of the thermal ridge evident in Fig. 14a but was partly an artifact of spatial variation of the $\hat{\mathbf{n}}$ unit vector resulting in a contribution to $\nabla \cdot \mathbf{Q}_n$ by $\hat{\mathbf{n}}$ convergence (not shown) in that region. A similar circumstance characterized the other two cases in the eastern portion of the thermal ridge. Conspicuously absent from Fig. 14d is any significant forcing in the vicinity of the trowal. It is evident that the predominant, column-averaged Q-G forcing for ascent in the occluded quadrant of this cyclone was associated with synoptic-scale (wave scale) processes, not with processes occurring on the scale of the individual baroclinic zones.

c. 7 November 1996

The Trenberth forcing function in the 500–900-hPa layer at 1200 UTC 7 November 1996 is shown in Fig. 15a. Three regions of fairly large forcing are evident; one centered over Milwaukee, Wisconsin, a fairly band-

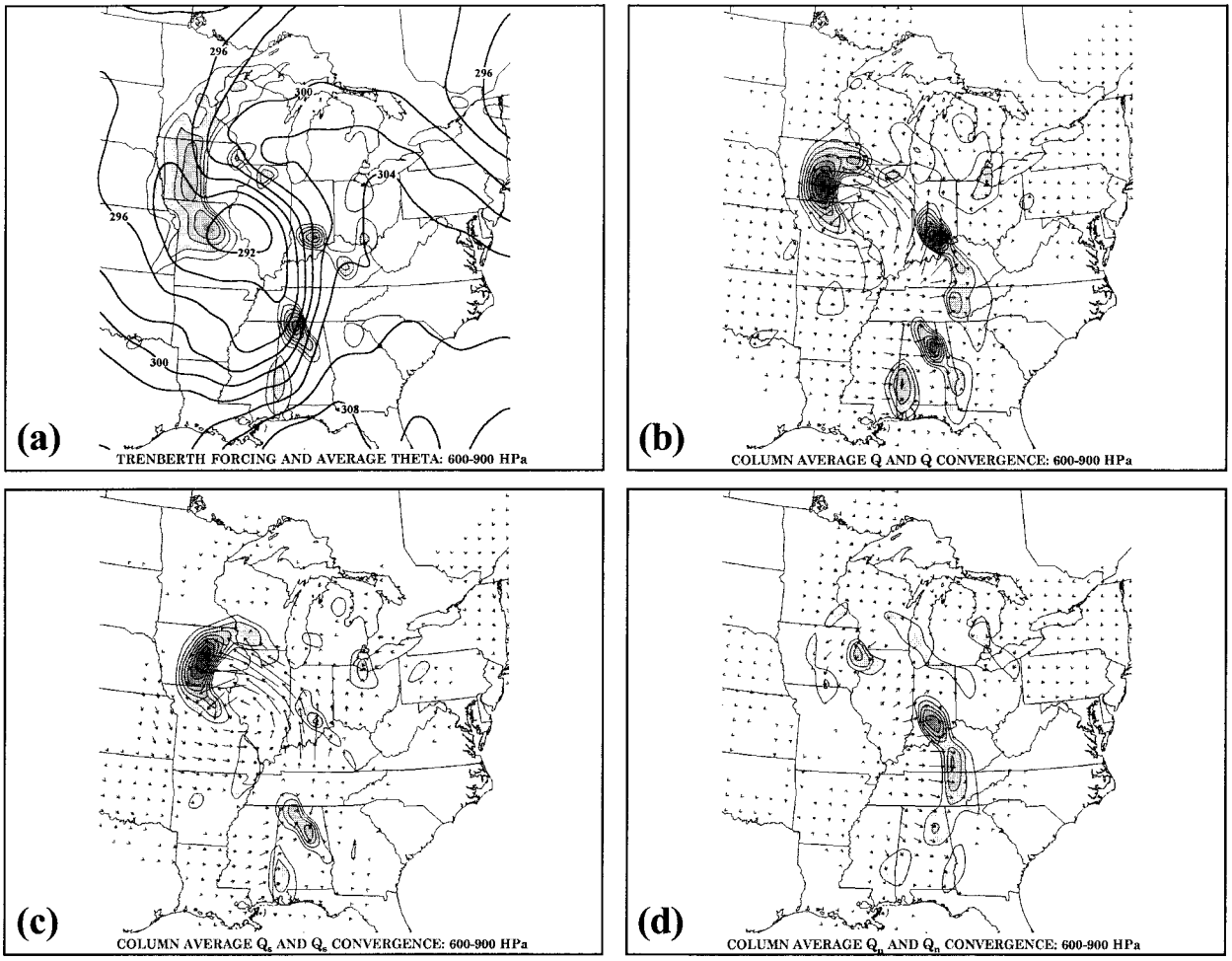

FIG. 14. (a) Column-averaged Trenberth forcing function (see text for explanation) and layer-averaged isentropes in the 600–900-hPa layer from an 18-h forecast of the UW-NMS valid at 0600 UTC 23 October 1996. Trenberth forcing function contoured and shaded in units of m kg^{-1} s^{-1} every 5×10^{-16} m kg^{-1} s^{-1} beginning at 5×10^{-16} m kg^{-1} s^{-1}. Layer-averaged isentropes (thick solid lines) labeled in K and contoured every 2 K. (b) Column-averaged **Q** vectors and **Q** vector convergence from an 18-h forecast of the UW-NMS valid at 0600 UTC 23 October 1996. Here **Q** convergence contoured and shaded in units of m kg^{-1} s^{-1} every 5×10^{-16} m kg^{-1} s^{-1} beginning at 5×10^{-16} m kg^{-1} s^{-1}. (c) As in (b) except for $\mathbf{Q}_s$. (d) As in (b) except for $\mathbf{Q}_n$.

ed feature extending southward from southeastern Ontario to near Cleveland, Ohio, and an area of significant forcing in northwest Ontario, coincident with the western half of the axis of maximum 500–900-hPa column-averaged θ. This last region was located just south and east of the trowal as identified in Fig. 7a.

A more complete accounting of the forcing function in the Q-G omega equation is shown in the 500–900-hPa column-averaged **Q** vectors and their convergence (Fig. 15b). The major forcing regions identified in Fig. 15a are also evident in the **Q**-vector convergence field although they are more sharply delineated. The trowal (approximately located along the axis of the thermal ridge in Fig. 15a) was an axis of robust forcing for vertical motion along its entire length, especially on its western end.

Fields of convergence of the partitioned **Q** vector provide further insight into the nature of the forcing responsible for the ascent in the occluded quadrant of the cyclone. The component $\mathbf{Q}_s$ and its convergence in the 500–900-hPa layer are shown in Fig. 15c. The distribution of this component of the **Q**-vector forcing resembles the synoptic-scale forcing (Fig. 15a), particularly in the western portion of the trowal, and is negligibly influenced by changes in the $\hat{\mathbf{s}}$ direction. As in the previous case, the axis of maximum $\mathbf{Q}_s$ forcing lies just south and east of the trowal. The near absence of $\mathbf{Q}_s$ forcing from just north of Lake Huron to northwest Ohio (along the lower-tropospheric cold frontal zone) demonstrates that $\mathbf{Q}_s$ convergence does not resolve Q-G vertical motions forced by frontal processes.

The $\mathbf{Q}_n$ field and its convergence in the 500–900-hPa layer at 1200 UTC 7 November are shown in Fig. 15d. The narrow, banded region of forcing coincident with

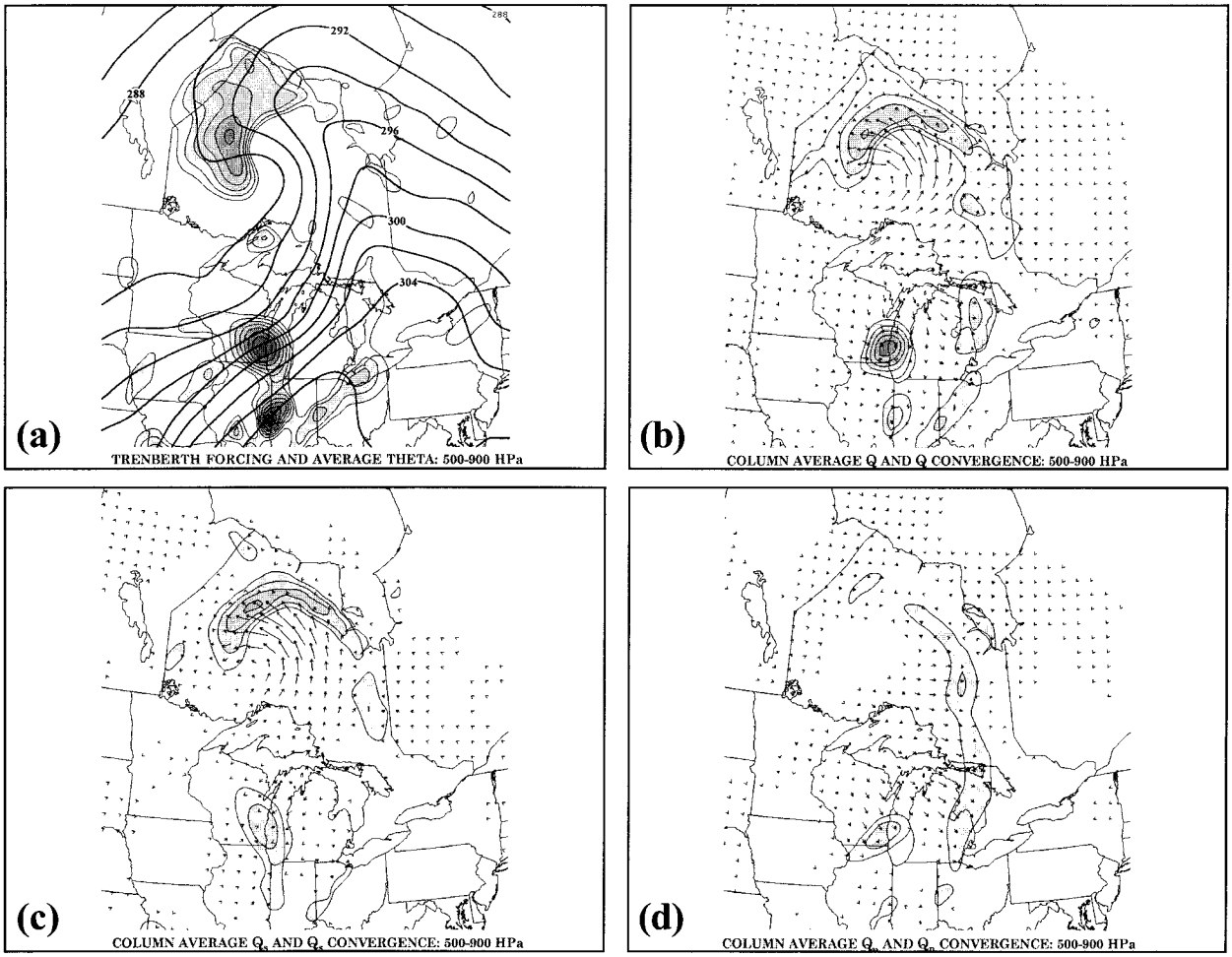

FIG. 15. (a) As for Fig. 14a except from a 12-h forecast of UW-NMS valid at 1200 UTC 7 November 1996 in the 500–900-hPa layer. (b) As for Fig. 14b except from a 12-h forecast of UW-NMS valid at 1200 UTC 7 November 1996 in the 500–900-hPa layer. (c) As for Fig. 14c except from a 12-h forecast of UW-NMS valid at 1200 UTC 7 November 1996 in the 500–900-hPa layer. (d) As for Fig. 14d except from a 12-h forecast of UW-NMS valid at 1200 UTC 7 November 1996 in the 500–900-hPa layer.

the cold frontal zone is particularly evident. The near absence of $\mathbf{Q}_n$ forcing in the vicinity of the trowal (except just west of James Bay in the weak southeastern portion of the thermal ridge) is also conspicuous and supports the implication made based on examination of the 23 October case; namely, that the Q-G forcing for vertical motion in the occluded quadrant of cyclones is predominantly a result of synoptic-scale processes, not frontal processes.

d. 1 April 1997

The Trenberth Q-G forcing in the 500–900-hPa layer at 0600 UTC 1 April 1997, along with the column-averaged isentropes in that layer, are shown in Fig. 16a (note the contour interval for the former is changed from that used in Figs. 14 and 15). One area of significant forcing is apparent stretching from south of Nova Scotia southwestward to east of the Delmarva Peninsula. This region of forcing, and a weaker eastern extension, were located in the vicinity of the trowal in this cyclone. The column-averaged **Q** vectors and their convergence field are shown in Fig. 16b. The **Q**-vector convergence field identifies the same regions of forcing as in Fig. 16a and in addition identifies the forcing along the primary and secondary cold fronts. A strip of fairly weak forcing east of the Carolina coast appears associated with the secondary baroclinic zone, whereas only discontinuous regions of forcing to the east along the primary cold front are evident.

Partitioning of the column-averaged **Q**-vector forcing reveals the same result as in the previous cases. The $\mathbf{Q}_s$ component and its convergence are shown in Fig. 16c. The only feature in the field of convergence of $\mathbf{Q}_s$ bears a resemblance to the traditional Q-G forcing and is concentrated just south of the trowal in the occluded quadrant. The $\mathbf{Q}_n$ component (Fig. 16d) is strongest in the eastern portion of the trowal and southeast of Nova

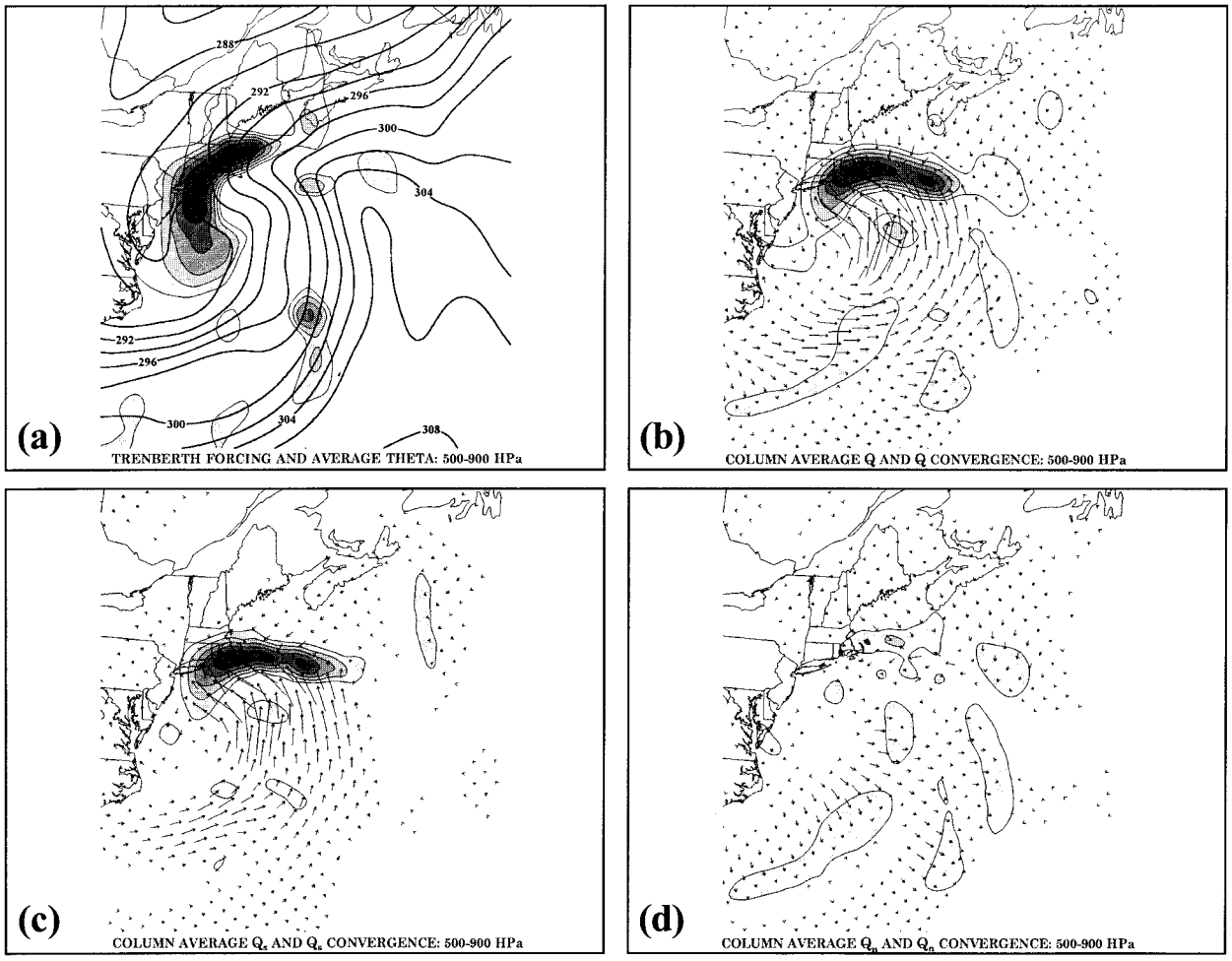

FIG. 16. (a) As for Fig. 15a except from an 18-h forecast of the UW-NMS valid at 0600 UTC 1 April 1997 with Trenberth forcing contoured and shaded every 10×10^{-16} m kg^{-1} s^{-1} beginning with 5×10^{-16} m kg^{-1} s^{-1}. (b) As for Fig. 15b except from an 18-h forecast of the UW-NMS valid at 0600 UTC 1 April 1997 with **Q** convergence contoured and shaded every 10×10^{-16} m kg^{-1} s^{-1} beginning with 5×10^{-16} m kg^{-1} s^{-1}. (c) As for Fig. 15c except from an 18-h forecast of the UW-NMS valid at 0600 UTC 1 April 1997 with $\mathbf{Q}_s$ convergence contoured and shaded every 10×10^{-16} m kg^{-1} s^{-1} beginning with 5×10^{-16} m kg^{-1} s^{-1}. (d) As for Fig. 15d except from an 18-h forecast of the UW-NMS valid at 0600 UTC 1 April 1997 with $\mathbf{Q}_n$ convergence contoured and shaded every 10×10^{-16} m kg^{-1} s^{-1} beginning with 5×10^{-16} m kg^{-1} s^{-1}.

Scotia in an area corresponding to the warm frontal region of the cyclone. The other significant $\mathbf{Q}_n$-forcing regions are located off of the Carolina coast and correspond to portions of the primary and secondary lower-tropospheric cold frontal zones associated with this cyclone. Interestingly, the thermal ridge described by the column-averaged 306 K isentrope (Fig. 16a) is also a significant $\mathbf{Q}_n$-convergence maximum along the primary cold front.

The degree of similarity among the three cases presented here suggests that the Q-G forcing for vertical motion in the occluded quadrant of cyclones is not accounted for by traditional Q-G frontogenesis along the component baroclinic zones constituting the occluded structure. Instead, ascent in this sector of the cyclone is predominantly a result of dynamical forcing that operates on the scale of the disturbance. This forcing is directly related to the rotational component of the vector frontogenesis function.

The considerable similarity between the distribution and magnitude of the Trenberth forcing for Q-G vertical motion and that of the $\mathbf{Q}_s$ forcing is not limited to the cases described here and is worthy of note as it bears on the nature of the occlusion process. In their vector generalization of the traditional Petterssen frontogenetic function Keyser et al. (1988) described the vector frontogenesis function as

$$\mathbf{F} = F_n\hat{\mathbf{n}} + F_s\hat{\mathbf{s}}, \tag{9}$$

which can be translated directly, at the level of quasi-geostrophic theory, in a form that employs the **Q** vector, to

$$\mathbf{Q} = Q_n\hat{\mathbf{n}} + Q_s\hat{\mathbf{s}}. \tag{10}$$

Following Keyser et al. (1988), in which F_n and F_s were defined, we define Q_n and Q_s consistent with our slightly different definition of $\hat{\mathbf{n}}$, to be

$$Q_n = \frac{f_o\gamma}{2}|\nabla\theta|(E\cos 2\beta) \quad \text{and}$$

$$Q_s = \frac{f_o\gamma}{2}|\nabla\theta|(\zeta_g + E\sin 2\beta), \tag{11}$$

where $\hat{\mathbf{n}} = \nabla\theta/|\nabla\theta|$ and $\hat{\mathbf{s}} = \hat{\mathbf{k}} \times \nabla\theta/|\nabla\theta|$. Here, E is the resultant geostrophic deformation and β is the angle between the isentropes and the local axis of dilatation. Given these relationships, the $\mathbf{Q}_s$ component of the Q-G forcing of vertical motion becomes,

$$\begin{aligned} -2\nabla\cdot\mathbf{Q}_s &= -2f_o\gamma\nabla\cdot(Q_s\hat{\mathbf{s}}) \\ &= -f_o\gamma\nabla\cdot\left\{[|\nabla\theta|(\zeta_g + E\sin 2\beta)]\left[\frac{\hat{\mathbf{k}}\times\nabla\theta}{|\nabla\theta|}\right]\right\} \\ -2\nabla\cdot\mathbf{Q}_s &= -f_o\gamma[\hat{\mathbf{k}}\times\nabla\theta]\cdot\nabla(\zeta_g + E\sin 2\beta). \end{aligned} \tag{12}$$

Equation (12) can be split into two terms, A and B, for analysis:

$$\begin{aligned} &-2\nabla\cdot\mathbf{Q}_s \\ &\quad = \underbrace{-f_o\gamma[\hat{\mathbf{k}}\times\nabla\theta]\cdot\nabla\zeta_g}_{\text{A}} \underbrace{-f_0\gamma[\hat{\mathbf{k}}\times\nabla\theta]\cdot\nabla E\sin 2\beta}_{\text{B}}. \end{aligned} \tag{13}$$

Term A in (13) reduces to a familiar form since the cross product portion of it in component form is equal to

$$\hat{\mathbf{k}}\times\nabla\theta = \left(-\frac{\partial\theta}{\partial y}\hat{\mathbf{i}} + \frac{\partial\theta}{\partial x}\hat{\mathbf{j}}\right),$$

which can be converted into a relationship for the thermal wind components

$$\frac{1}{\gamma}\frac{\partial U_g}{\partial p} = \frac{\partial\theta}{\partial y} \quad \text{and} \quad \frac{-1}{\gamma}\frac{\partial V_g}{\partial p} = \frac{\partial\theta}{\partial x}.$$

Thus, term A in (13) becomes

$$\text{A} = f_o\mathbf{V}_\text{T}\cdot\nabla\zeta_g, \tag{14}$$

which is precisely half of (2), the forcing function in the Trenberth (1978) approximate version of the Q-G omega equation, a result suggested by Kurz (1992). One obvious consequence of the preceding derivation is that the vector $\mathbf{Q}_{\text{TR}}$ has real physical significance; namely, it describes *twice* the effect of the geostrophic relative vorticity on the rotation of $\nabla\theta$.

By analogy, term B in (13) is equal to

$$\text{B} = f_o\mathbf{V}_\text{T}\cdot\nabla(E\sin 2\beta). \tag{15}$$

Martin (1998c) has recently shown that the middle tropospheric deformation forcing for ascent (a portion of which is represented by term B) is small in nonfrontal regions *except* in the vicinity of thermal troughs and ridges accompanied by horizontal variations in the geostrophic flow. Thus, in general, $-2\nabla\cdot\mathbf{Q}_s$ will closely resemble the approximate Trenberth forcing for ascent in the middle troposphere. In the occluded thermal ridge, however, term B can be comparable to term A. In the three cases examined here, that was indeed the case (not shown), suggesting that the thermal gradient rotation required for the development of occluded structures is dependent on both the vorticity and the deformation of the flow.

5. Discussion

a. Quasigeostrophic forcing of ascent in the occluded quadrant

Extratropical cyclones often contain two significant frontal baroclinic zones; the cold front and the warm front. The evolution of the thermal structure of cyclones is the integrated result of changes both in the vigor of each baroclinic zone as well as in the orientation of the baroclinic zones with respect to one another, both of which occur continuously throughout the cyclone life cycle. Keyser et al. (1988) referred to these two processes as the components of a generalized vector frontogenesis function. Changes in the intensity of baroclinic zones are controlled by the process of traditional frontogenesis, which modulates the magnitude of the potential temperature gradient and operates on the scale of the individual baroclinic zone. This process is dynamically linked to the production of the banded vertical motions commonly associated with fronts (Sawyer 1956; Eliassen 1962). The geostrophic contribution to frontogenesis is described by the $\mathbf{Q}_n$ component of $\mathbf{Q}$.

Changes in the orientation of the frontal zones with respect to one another are a result of the rotational component of the vector frontogenesis function, which rotates the potential temperature gradient vector. This study suggests that the characteristic occluded thermal ridge, exhibited by each of the three storms reviewed in this paper, is produced by differential rotation of the warm and cold frontal baroclinic zones about the geopotential (sea level pressure) minimum during the cyclone life cycle. The geostrophic contribution to the vector rotation of $\nabla_p\theta$ is described by the $\mathbf{Q}_s$ component of the partitioned $\mathbf{Q}$ vector. The present case demonstrates that convergence of $\mathbf{Q}_s$ along straight isentropes will kink them at the point of maximum convergence, creating a thermal ridge in the horizontal (see Fig. 13). This same convergence of $\mathbf{Q}_s$ represents the predominant portion of the total forcing for Q-G vertical motion in the occluded quadrant of cyclones (Figs. 14, 15, and 16). Thus, the rotational component of the Q-G vector frontogenesis function, represented by the $\mathbf{Q}_s$ forcing, is found to be the underlying dynamical mechanism responsible for creating the occluded thermal structure

and for forcing the ascent associated with that process in the occluded quadrant of cyclones.

In their investigation of an idealized cyclone, Keyser et al. (1988) suggested that the rotational component of the vector frontogenesis function is controlled by dynamical processes that operate on the scale of the disturbance within which the individual frontal zones are embedded (i.e., the synoptic scale). Consistent with this suggestion, and a similar one made by Keyser et al. (1992), the analyses presented here demonstrate that the $\mathbf{Q}_s$ forcing is fundamentally a *synoptic-scale* forcing. Evidence for this assertion lies in the similarity, in magnitude and distribution, between the $\mathbf{Q}_s$ ($-2\boldsymbol{\nabla} \cdot \mathbf{Q}_s$) and the traditional Sutcliffe/Trenberth forcing (F_{TR}) for Q-G vertical motion in every case. Further, it was shown that the vorticity component of $\mathbf{Q}_s$ [term A in (13)] is precisely equal to one-half of $\mathbf{Q}_{TR}$, the vector expression in (3). As a consequence of their orientation parallel to the isentropes neither the Trenberth ($\mathbf{Q}_{TR}$) or $\mathbf{Q}_s$ forcings can produce regions of banded vertical motion parallel to baroclinic zones such as occur at fronts. In fact, it was found that a very small contribution to ascent in the occluded quadrant was associated with $-2\boldsymbol{\nabla} \cdot \mathbf{Q}_n$, the frontal-scale forcing, and that, when present, this forcing operated on the eastern end of the trowal (i.e., in the least developed portion of the thermal ridge). Additionally, this meager forcing was found to result partly from the convergence of the $\hat{\mathbf{n}}$ unit vector into the thermal ridge and not necessarily from Q-G frontogenesis.

Despite the numerous revisions that have been made to the original NCM, none have disagreed with the assertion that the occlusion process involves both the development of a thermal ridge and the ascent of warm sector air in the vicinity of the thermal ridge. Recent studies of occlusions have focused on the role played by frontogenesis in the development of the occluded thermal structure (e.g., Schultz and Mass 1993; Reed et al. 1994; Martin 1998a). The results presented here suggest that the evolution of the characteristic occluded thermal structure and the forcing of the attendant vertical motion are linked, not by a frontal-scale process, but by an underlying, *synoptic-scale* dynamical process. Based upon this result, it is suggested that further insight into the complicated process of occlusion is more likely to be achieved by ceasing to view it as a traditional frontal-scale process.

b. The trowal airstream

The use of isentropic relative flow analysis to describe the three-dimensional airflow through cyclones and to account for the distribution of clouds and precipitation began with the work of Namias (1939). He identified an airflow that originated in the warm sector boundary layer and ascended in two streams; one cyclonically to the west and one anticyclonically to the east. More recently, the same method has been employed by Browning and Harrold (1969), Harrold (1973), Carlson (1980), and Browning (1990). These studies suggested that the airflow through cyclones, and the corresponding cloud signatures of these storms, can be adequately described in terms of the behavior of three coherent airstreams; namely the warm conveyor belt (WCB), the cold conveyor belt (CCB), and the dry airstream. The WCB is a stream of air that flows poleward east of the surface cold front and rises anticyclonically over the surface warm front, forming the eastern portion of the comma head cloud shield characteristic of extratropical cyclones. The CCB originates in the easterly flow poleward of the surface warm front, undercuts the WCB flow, and travels westward toward the surface cyclone center. Upon approach to the sea level pressure minimum, the CCB begins a gradual ascent to the west before turning anticyclonically to the north. This ascent is considered largely responsible for producing the observed cloudiness and precipitation in the occluded quadrant of the cyclone. Generally, ascent in the CCB is not as vigorous as in the WCB. In fact, the cloud associated with the CCB is mainly confined to low and medium levels (Browning 1990). Such a scenario strongly suggests that the comma head is a result of modest ascent of cool, moist air in the CCB and is not related to the significant ascent of warm sector air characteristic of the process of occlusion.

Other studies employing isentropic relative flow analysis have offered explanations for the distribution of clouds and precipitation that differ from that of the cold conveyor belt model. In their investigation of the mesoscale circulation and precipitation distribution in an occluded cyclone, Atkinson and Smithson (1974) illustrated cyclonically ascending, warm sector-based trajectories that contributed to a precipitation event over southwest England. In his investigation of a nondeepening cyclone, Iskenderian (1988) showed a flow of warm moist air transported northward from the Gulf of Mexico between 700 and 500 hPa that bifurcated east of the cyclone center. A portion of this flow curved cyclonically and ascended to the north and west of the surface low center whereas the other portion ascended anticyclonically and moved east of the low center (his Fig. 7). The cyclonically ascending airstreams identified in these studies were responsible for producing the clouds and precipitation observed in the western extension of the cyclone comma head.

More recently, numerical model-based studies of occluded cyclones have offered a more refined and detailed picture of the airflow through the cyclone and the development of clouds and precipitation in the occluded quadrant (e.g., Kurz 1988a; Mass and Schultz 1993; Schultz and Mass 1993; Reed et al. 1994; Martin 1998b). These studies have revealed that the airflow in cyclones is often more complicated than that portrayed in the conveyor belt model. Interestingly, an element common to all of these simulations is the presence of

a stream of warm sector, boundary layer air that ascends cyclonically into the occluded quadrant of the storm.

Kurz (1988a) related the typical cloud distribution in an occluded cyclone to elements of the classical occlusion model. He noted that near the end of the development phase the ascent in the WCB acquired significant cyclonic vorticity such that a large portion of that airstream ascended cyclonically (his Fig. 4b) in the occluded stage of the life cycle. This cyclonically turning ascent was related to the ''cloud spiral'' (comma head) characteristic of the northwest quadrant of occluded cyclones.

In their numerical simulation of an occluded continental cyclone, Mass and Schultz (1993) also identified a significant cyclonically ascending airstream (their Fig. 18) that originated in the warm sector. Reed et al. (1994), in a ''quasi-ideal'' simulation of the ERICA IOP-4 storm, identified a cyclonically ascending airstream that originated in the warm sector (their Figs. 10, 11b). This airstream was largely responsible for producing the western extension of the comma head that characterized that storm. Wernli (1997), using coherent ensembles of trajectories (CET's) to identify airstreams in model simulations, has also reported the presence of this cyclonically ascending warm sector airstream (see the CET labeled ''Y'' in his Fig. 3a). Rotunno et al. (1994) noted the cyclonic ascent of parcels through a trowal-like structure in their examination of frontogenesis in an idealized numerical model (see their Figs. 16 and 17).

In each case presented here, rapid cyclonic ascent of warm sector air, to nearly 7 km in some cases, occurred along the trowal and was responsible for significant cloud and precipitation production. Following Martin (1998b), we have termed this airstream the ''trowal airstream'' as a result of its spatial relationship to the trowal structure. The current study is not the first to identify this important cloud and precipitation producing airstream, as the foregoing discussion indicates. It is, however, the first to directly relate it to the three-dimensional occluded structure and, more importantly, to the dynamical forcing that supports its ascent in the occluded quadrant of cyclones. The current analysis also supports the aforementioned investigations in suggesting that the western extension of the cyclone comma head cloud shield sometimes results from cyclonically rising warm sector air and is not entirely accounted for by a single anticyclonically rising cool sector airstream (with origins poleward of the surface warm front) as suggested in the cold conveyor belt model.

6. Summary and conclusions

Numerical model-based analyses of the structure and dynamics of, and airflow through, the occluded quadrant of three extratropical cyclones has been presented. It is shown that the three-dimensional trowal structure is easily identifiable in model output given emerging visualization technologies. In each of the three cyclones investigated, significant cyclonically turning ascent of air, which originated in the warm sector boundary layer, occurred in the occluded quadrant of the cyclone and exhibited an intriguing spatial relationship to the trowal. This previously identified, cyclonically ascending airstream represents a major cloud and precipitation producing flow in occluded cyclones and is designated here as the *trowal airstream.* The trowal airstream is often responsible for the production of so-called wrap-around precipitation to the north and west of the occluded surface cyclone center.

Quasigeostrophic forcing of the vertical motion that supports the trowal airstream was examined through consideration of the **Q** vector partitioned into natural coordinate components along $\mathbf{Q}_s$ isentropes and across $\mathbf{Q}_n$ isentropes on isobaric surfaces representing the *rotational* and *magnitude* components of the Q-G vector frontogenesis function, respectively. The geostrophic contribution to the formation of the characteristic thermal structure of occluded cyclones (i.e., a narrow thermal ridge) is shown to be accomplished by $\mathbf{Q}_s$; more specifically by a convergent field of $\mathbf{Q}_s$. The convergence of $\mathbf{Q}_s$ also provides the predominant forcing for Q-G vertical motion in the occluded quadrant of such storms and supports the ascent of the trowal airstream.

A well-understood physical link exists between traditional frontogenesis and the production of vertical circulations associated with warm and cold frontal zones. The findings described here represent a conceptual analog that relates *rotational* frontogenesis to the production of vertical motions in occluded frontal regions. The fact that rotational frontogenesis and not traditional (magnitude) frontogenesis is central to the dynamics of the occluded quadrant suggests a fundamental difference between the processes of ''occludogenesis'' and traditional frontogenesis. This emerging view is supported by the fact that a considerable similarity was found, in magnitude, horizontal distribution, and mathematical form between the $\mathbf{Q}_s$ forcing and the traditional Sutcliffe/Trenberth forcing for Q-G vertical motion pointing to the predominance of synoptic-scale processes in forcing ascent and structural evolution in the occluded quadrant of cyclones. The results of this analysis therefore suggest that traditional frontogenetic processes play a subordinate role in forcing Q-G vertical motions and in effecting three-dimensional structural changes in the occluded sector of postmature-phase midlatitude cyclones.

Acknowledgments. The suggestions of Prof. Dan Keyser and comments from two anonymous reviewers served to improve the presentation of this work. The research was supported by the National Science Foundation under Grant ATM-9505849.

REFERENCES

Atkinson, B. W., and P. A. Smithson, 1974: Meso-scale circulations and rainfall patterns in an occluding depression. *Quart. J. Roy. Meteor. Soc.*, **100,** 3–22.

Barnes, S. L., and B. R. Colman, 1993: Quasigeostrophic diagnosis of cyclogenesis associated with a cutoff extratropical cyclone—The Christmas 1987 storm. *Mon. Wea. Rev.,* **121,** 1613–1634.

Bjerknes, J., and H. Solberg, 1922: Life cycle of cyclones and the polar front theory of atmospheric circulation. *Geofys. Publ.,* **3,** 1–18.

Browning, K., 1990: Organization of clouds and precipitation in extratropical cyclones. *Extratropical Cyclones: The Erik Palmén Memorial Volume,* C. W. Newton and E. O. Holopainen, Eds., Amer. Meteor. Soc., 129–151.

——, and T. W. Harrold, 1969: Air motion and precipitation growth in a wave depression. *Quart. J. Roy. Meteor. Soc.,* **95,** 288–309.

Carlson, T. N., 1980: Airflow through midlatitude cyclones and the comma cloud pattern. *Mon. Wea. Rev.,* **108,** 1498–1509.

Chen, C., and W. R. Cotton, 1983: A one-dimensional simulation of the stratocumulus capped mixed layer. *Bound.-Layer Meteor.,* **25,** 289–321.

Cotton, W. R., G. J. Tripoli, R. M. Rauber, and E. A. Mulvihill, 1986: Numerical simulation of the effects of varying ice crystal nucleation rates and aggregation processes on orographic snowfall. *J. Climate Appl. Meteor.,* **25,** 1658–1680.

Crocker, A. M., W. L. Godson, and C. M. Penner, 1947: Frontal contour charts. *J. Meteor.,* **4,** 95–99.

Eliassen, A., 1962: On the vertical circulation in frontal zones. *Geofys. Publ.,* **24,** 147–160.

Emanuel, K. A., 1991: A scheme for representing cumulus convection in large-scale models. *J. Atmos. Sci.,* **48,** 2313–2335.

Flatau, P., G. J. Tripoli, J. Verlinde, and W. R. Cotton, 1989: The CSU RAMS cloud microphysical module: General theory and code documentation. Tech. Rep. 451, Dept. of Atmospheric Science, Colorado State University, 88 pp. [Available from Dept. of Atmospheric Science, Colorado State University, Fort Collins, CO 80523.]

Galloway, J. L., 1958: The three-front model: Its philosophy, nature, construction and use. *Weather,* **13,** 3–10.

——, 1960: The three-front model, the developing depression and the occluding process. *Weather,* **15,** 293–309.

Godson, W. L., 1951: Synoptic properties of frontal surfaces. *Quart. J. Roy. Meteor. Soc.,* **77,** 633–653.

Harrold, T. W., 1973: Mechanisms influencing the distribution of precipitation within baroclinic disturbances. *Quart. J. Roy. Meteor. Soc.,* **99,** 232–251.

Holton, J. R., 1992: *An Introduction to Dynamical Meteorology.* 3d ed. Academic Press, 511 pp.

Hoskins, B. J., and M. A. Pedder, 1980: The diagnosis of middle latitude synoptic development. *Quart. J. Roy. Meteor. Soc.,* **106,** 707–719.

——, I. Draghici, and H. C. Davies, 1978: A new look at the ω-equation. *Quart. J. Roy. Meteor. Soc.,* **104,** 31–38.

Iskenderian, H., 1988: Three-dimensional airflow and precipitation structure in a nondeepening cyclone. *Wea. Forecasting,* **3,** 18–32.

Jewell, R., 1981: Tor Bergeron's first year in the Bergen School: Towards an historical appreciation. *Weather and Weather Maps: A Volume Dedicated to the Memory of Tor Bergeron.* Vol. 10, *Contributions to Current Research in Geophysics,* G. H. Lilequist, Ed., Birkhauser Verlag, 474–490.

Keyser, D., M. J. Reeder, and R. J. Reed, 1988: A generalization of Petterssen's frontogenesis function and its relation to the forcing of vertical motion. *Mon. Wea. Rev.,* **116,** 762–780.

——, B. D. Schmidt, and D. G. Duffy, 1992: Quasigeostrophic vertical motions diagnosed from along- and cross-isentrope components of the Q vector. *Mon. Wea. Rev.,* **120,** 731–741.

Kurz, M., 1988a: Development of cloud distribution and relative motions during the mature and occlusion stage of a typical cyclone development. Preprints, *Palmén Memorial Symp. on Extratropical Cyclones,* Helsinki, Finland, Amer. Meteor. Soc., 201–204.

——, 1988b: Intercorrelations between cyclogenesis and frontogenesis during a typical development in the westerlies. Preprints, *Palmén Memorial Symp. on Extratropical Cyclones,* Helsinki, Finland, Amer. Meteor. Soc., 223–226.

——, 1992: Synoptic diagnosis of frontogenetic and cyclogenetic processes. *Meteor. Atmos. Phys.,* **48,** 77–91.

Martin, J. E., 1998a: The structure and evolution of a continental winter cyclone. Part I: Frontal structure and the classical occlusion process. *Mon. Wea. Rev.,* **126,** 303–328.

——, 1998b: The structure and evolution of a continental winter cyclone. Part II: Frontal forcing of an extreme snow event. *Mon. Wea. Rev.,* **126,** 329–347.

——, 1998c: On the deformation term in the quasigeostrophic omega equation. *Mon. Wea. Rev.,* **126,** 2000–2007.

Mass, C. F., and D. M. Schultz, 1993: The structure and evolution of a simulated midlatitude cyclone over land. *Mon. Wea. Rev.,* **121,** 889–917.

Morris, R. M., 1972: The trowal, an important feature of frontal analysis. *Meteor. Mag.,* **101,** 150–153.

Namias, J., 1939: The use of isentropic analysis in short term forecasting. *J. Aeronaut. Sci.,* **6,** 295–298.

National Climatic Data Center, 1996: *Storm Data.* Vol. 38, No. 10, 135 pp. [Available from National Climatic Data Center, Asheville, NC 28801.]

——, 1997a: *Storm Data.* Vol. 39, No. 3, 169 pp. [Available from National Climatic Data Center, Asheville, NC 28801.]

——, 1997b: *Storm Data.* Vol. 39, No. 4, 206 pp. [Available from National Climatic Data Center, Asheville, NC 28801.]

Penner, C. M., 1955: A three-front model for synoptic analyses. *Quart. J. Roy. Meteor. Soc.,* **81,** 89–91.

Reed, R. J., Y.-H. Kuo, and S. Low-Nam, 1994: An adiabatic simulation of the ERICA IOP 4 storm: An example of quasi-ideal frontal cyclone development. *Mon. Wea. Rev.,* **122,** 2688–2708.

Rotunno, R., W. C. Skamarock, and C. Snyder, 1994: An analysis of frontogenesis in numerical simulations of baroclinic waves. *J. Atmos. Sci.,* **51,** 3373–3398.

Sadourny, R., 1975: The dynamics of finite-difference models of the shallow-water equations. *J. Atmos. Sci.,* **32,** 680–689.

Sawyer, J. S., 1956: The vertical circulation at meteorological fronts and its relation to frontogenesis. *Proc. Roy. Soc. London,* **234A,** 346–362.

Schultz, D., and C. Mass, 1993: The occlusion process in a midlatitude cyclone over land. *Mon. Wea. Rev.,* **121,** 918–940.

Sutcliffe, R. C., 1947: A contribution to the problem of development. *Quart. J. Roy. Meteor. Soc.,* **73,** 370–383.

Tremback, C. J., and R. Kessler, 1985: A surface temperature and moisture parameterization for use in mesoscale numerical models. Preprints, *Seventh Conf. on Numerical Weather Prediction,* Montreal, PQ, Canada, Amer. Meteor. Soc., 355–358.

——, J. Powell, W. R. Cotton, and R. A. Pielke, 1987: The forward-in-time upstream advection scheme: Extension to higher orders. *Mon. Wea. Rev.,* **115,** 540–555.

Trenberth, K. E., 1978: On the interpretation of the diagnostic quasi-geostrophic omega equation. *Mon. Wea. Rev.,* **106,** 131–137.

Tripoli, G. J., 1992a: An explicit three-dimensional nonhydrostatic numerical simulation of a tropical cyclone. *Meteor. Atmos. Phys.,* **49,** 229–254.

——, 1992b: A nonhydrostatic numerical model designed to simulate scale interaction. *Mon. Wea. Rev.,* **120,** 1342–1359.

Wernli, H., 1997: A Lagrangian-based analysis of extratropical cyclones. Part II: A detailed case study. *Quart. J. Roy. Meteor. Soc.,* **123,** 1677–1706.